© 2022. Published by The Company of Biologists Ltd | Journal of Experimental Biology (2023) 226, jeb244949. doi:10.1242/jeb.244949

RESEARCH ARTICLE

One size does not fit all: diversity of length–force properties of obliquely striated muscles

Joseph T. Thompson[1,*], Kari R. Taylor-Burt[1,2] and William M. Kier[3]

ABSTRACT

Obliquely striated muscles occur in 17+ phyla, likely evolving repeatedly, yet the implications of oblique striation for muscle function are unknown. Contrary to the belief that oblique striation allows high force output over extraordinary length ranges (i.e. superelongation), recent work suggests diversity in operating length ranges and length–force relationships. We hypothesize oblique striation evolved to increase length–force relationship flexibility. We predict that superelongation is not a general characteristic of obliquely striated muscles and instead that length–force relationships vary with operating length range. To test these predictions, we measured length–force relationships of five obliquely striated muscles from inshore longfin squid, *Doryteuthis pealeii*: tentacle, funnel retractor and head retractor longitudinal fibers, and arm and fin transverse fibers. Consistent with superelongation, the tentacle length–force relationship had a long descending limb, whereas all others exhibited limited descending limbs. The ascending limb at $0.6P_0$ was significantly broader (P<0.001) for the tentacle length–force relationship ($0.43\pm0.04L_0$; where L_0 is the preparation length that produced peak isometric stress, P_0) than for the arm ($0.29\pm0.03L_0$), head retractor ($0.24\pm0.06L_0$), fin ($0.20\pm0.04L_0$) and funnel retractor ($0.27\pm0.03L_0$). The fin's narrow ascending limb differed significantly from those of the arm (P=0.004) and funnel retractor (P=0.012). We further characterized the tentacle preparation's maximum isometric stress (315±78 kPa), maximum unloaded shortening velocity ($2.97\pm0.55L_0$ s^{-1}) and ultrastructural traits (compared with the arm), which may explain its broader length–force relationship. Comparison of obliquely striated muscles across taxa revealed length–force relationship diversity, with only two species exhibiting superelongation.

KEY WORDS: Squid, *Doryteuthis pealeii*, Superelongation, Force–velocity, Muscular hydrostats, Stagger angle

INTRODUCTION

Obliquely striated muscles are so called because the dense bodies (i.e. Z-elements) that anchor the thin myofilaments are aligned at an oblique angle to the long axis of the cell. This muscle type is absent from vertebrates and arthropods, occurring instead in the majority of soft-bodied invertebrate phyla that use hydrostatic skeletons for support and movement (Amsellem and Nicaise, 1980; Bone and Ryan, 1974; Bouligard, 1966; Carnevali et al., 1986; De Eguileor and Valvassori, 1977; Eakin and Brandenburger, 1974; Hanson and Lowy, 1961; Kuga and Matsuno, 1988; Matsuno and Kuga, 1989; Norenburg and Roe, 1998, 1974; Rieger and Mainitz, 1977; Rosenbluth, 1968, 1972; Ruppert, 1991; Teuchert, 1974; Turbeville and Ruppert, 1985; Ward et al., 1986). Details of the diversity of ultrastructure of these cells coupled with their phylogenetic distribution suggest that oblique striation evolved independently several times, presumably from a non-striated precursor (Paps et al., 2009; Prosser, 1979, 1982). In spite of their widespread occurrence and importance for soft-bodied invertebrates, we know relatively little about the function and significance of oblique striation.

The ultrastructure of obliquely striated muscle differs from that of cross-striated muscle. The thick and thin myofilaments of obliquely striated muscle, although aligned in parallel to the longitudinal axis of the fiber, are not arranged in register across the cell as in cross-striated fibers; the myofilaments are staggered in an oblique pattern (Fig. 1). Obliquely striated muscle lacks transverse banding and a distinct Z-disc is absent. Instead, the thin myofilaments are anchored to rows of dense bodies that are aligned at a small angle to the longitudinal axis of the fiber. This angle, termed the stagger angle (SA), increases as the fiber shortens and decreases as the fiber is elongated (see Fig. 1B–D for illustration). For example, in squid mantle and funnel retractor muscle, the stagger angle at rest was reported to be 6–12 deg, increasing to 60 deg if the glycerol-extracted muscle was treated with adenosine triphosphate (Hanson and Lowy, 1957). In addition to differences in the myofilament arrangement compared with cross-striated muscle, there are other differences in myofilament dimensions, the excitation–contraction coupling system, fiber size and mitochondrial distribution (Kier, 1985, 1996).

Oblique striation is commonly considered to be an adaptation that permits superelongation, i.e. the ability of striated muscle to operate over an extreme range of muscle lengths, much greater than could be accommodated by cross-striated fibers (Lanzavecchia, 1977; Lanzavecchia and Arcidiacono, 1981; Lanzavecchia and De Eguileor, 1976; Miller, 1975; Rosenbluth, 1967; 1968; Toida et al., 1975). For example, the overlap of thick and thin filaments in obliquely striated leech longitudinal body wall muscle can be maintained over a fivefold increase in body length (Lanzavecchia, 1977; Lanzavecchia and Arcidiacono, 1981; Lanzavecchia and De Eguileor, 1976) and Gerry and Ellerby (2011) showed that these muscle fibers produce nearly half of their peak isometric force at lengths approaching 2.5 times L_0, the length at which the muscle fibers produce maximum isometric force *in vitro*.

Other work, however, suggests that the properties of leech body wall muscle are not typical of the majority of obliquely striated fibers. First, the range of elongation and shortening of the obliquely striated muscles that have been studied varies widely and many

[1]Department of Biology, Franklin & Marshall College, Lancaster, PA 17604-3003, USA. [2]Department of Science, Mount St Mary's University, Emmitsburg, MD 21727, USA. [3]Department of Biology, University of North Carolina at Chapel Hill, Chapel Hill, NC 27599, USA.

*Author for correspondence (joseph.thompson@fandm.edu)

J.T.T., 0000-0003-0278-821X

Received 30 August 2022; Accepted 28 October 2022

Journal of Experimental Biology (2023) 226, jeb244949. doi:10.1242/jeb.244949

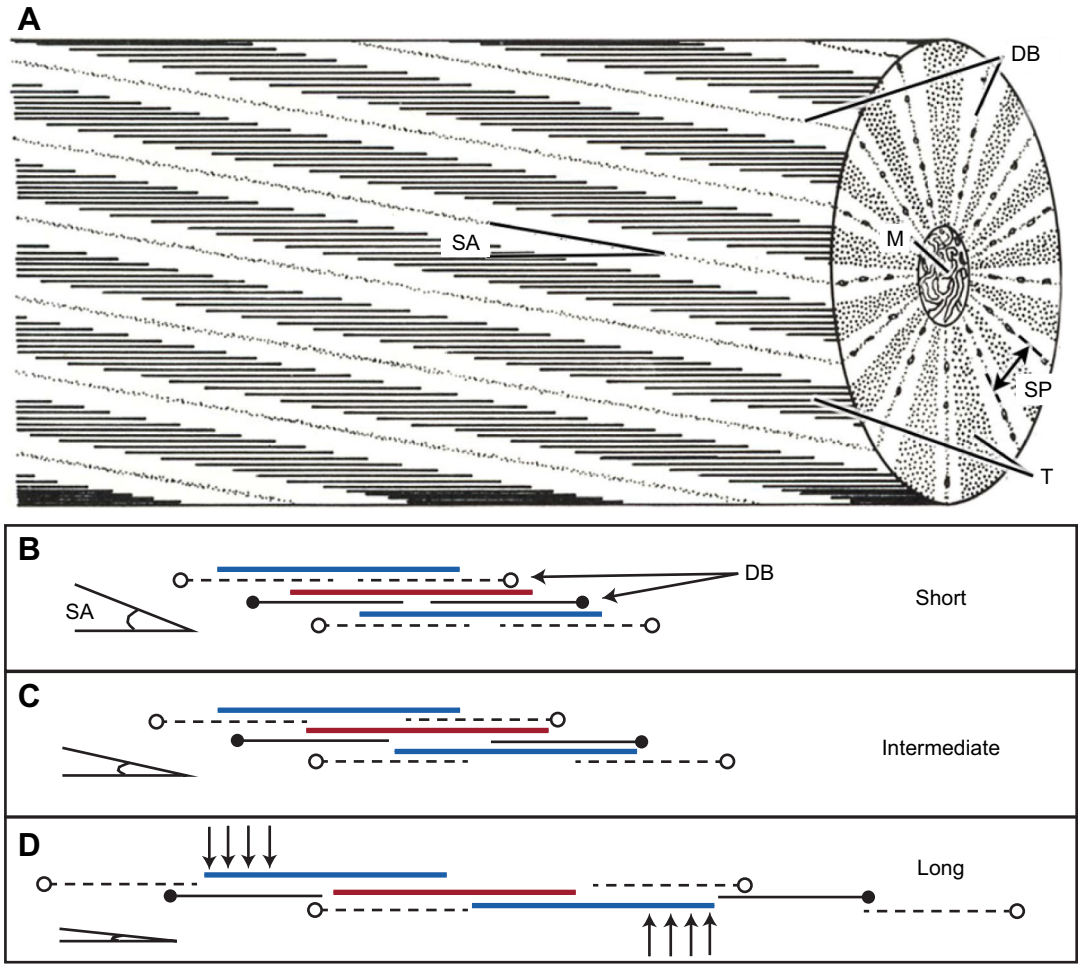

Fig. 1. Obliquely striated muscle. (A) Schematic diagram illustrating the arrangement of myofilaments in an obliquely striated muscle fiber. The thick filaments (T) are parallel to the longitudinal axis of the fiber in a staggered array surrounding a core containing the nucleus and mitochondria (M). The thin filaments (not shown) are anchored to dense bodies (DB), which are aligned at a small angle, the stagger angle (SA), to the longitudinal axis of the fiber. The spacing (SP) between the adjacent alignment of dense bodies as observed in cross-section is indicated. (Modified from Kier, 1985). (B–D) Schematic diagrams illustrating how SA and myofilament overlap decrease as muscle fiber length goes from short (B) to intermediate (C) to long (D). Different symbols, colors and patterns are used for alternate dense bodies and thick and thin filaments to make them easier to see. Arrows in D indicate the potential for a thick filament to interact with new thin filaments at long fiber lengths (see Discussion for details).

experience a relatively narrow operating range (e.g. Ort et al., 1974). Even in an individual animal, the operating range of the fibers from various muscles may vary widely, e.g. the tentacle and nuchal retractor muscles of the longfin squid *Doryteuthis pealeii* experience strains of 80% and 50%, respectively (Kier, 1982; Thompson et al., 2016), while the longitudinal fibers of the funnel retractor muscles experience strains that range from only 4% to 15% (Rosenbluth et al., 2010) and the transverse muscles of the arms function nearly isometrically (Kier, 1982).

In addition, the broad length–force relationship of leech body wall muscle is not representative of the majority of obliquely striated muscles that have been studied. For example, the circular muscles of the earthworm *Pheretima communissima* do not exhibit superelongation and instead have a much narrower length–force relationship (Hidaka et al., 1969), and a number of obliquely striated muscles of cephalopods have length–force relationships that are more typical of cross-striated fibers with no evidence of superelongation (Kier and Curtin, 2002; Milligan et al., 1997; Thompson et al., 2014; Zullo et al., 2022).

We hypothesize that obliquely striated muscle evolved in soft bodied invertebrates to allow adjustment of the length–force relationship to accommodate the operating length range of a muscle fiber. In the rigid skeleton and lever systems of arthropods and vertebrates, the relatively narrow operating length range of cross-striated muscle can lead to the evolution of a wide array of body and limb movements by either (1) altering the location of insertion on the skeleton, and thus the length of the input arm of the lever system (Biewener and Patek, 2018), or (2) altering the angle of pennation of the fibers in a muscle (Azizi et al., 2008). This adjustment is essential because only limited variation in length–force relationships has been observed in cross-striated fibers (Lieber and Ward, 2011) and there is limited sarcomere length change during movement (Burkholder and Lieber, 2001). Such adjustment is not possible with hydrostatic skeletons because they lack rigid lever systems. Instead, the muscle fibers must be altered during evolution to accommodate the range of length changes that occur during movement, as this range is determined by the shape and relative dimensions of the animal (or muscular hydrostatic organ) and the orientation of the muscle fibers in question. For example, vermiform animals often undergo large length changes and their longitudinal muscles must undergo identical changes in length. In contrast, their circular muscles shorten by a relatively small amount

to produce large elongation. The relative strains are a function simply of the geometry of the organism and the essentially constant volume of the animal (Kier, 2012).

Overview of experiments

The major goal of our investigation was to compare the length–force properties of several obliquely striated muscles from the inshore longfin squid, *Doryteuthis pealeii*. We anticipated that superelongation would not be a general characteristic of the obliquely striated muscles of *D. pealeii*. In addition, we predicted that the length–force relationship would vary proportionately with the strain (i.e. change in length divided by the resting length) experienced by the muscle *in vivo*.

We first characterized the contractile properties of the tentacle longitudinal muscle fibers because they are an example of a fiber type that operates over a large length range. We investigated the stimulus frequency–force and length–force properties of these fibers. Because these fibers have not been studied previously, we also characterized their force–velocity properties and maximum isometric stress, both of which have been shown previously to vary with myofilament dimensions (Kier and Curtin, 2002). Next, we investigated the length–force relationship of four additional muscles: the arm and fin transverse muscle fibers and the longitudinal fibers of both the head retractor and funnel retractor muscles. The length–force relationship of the arm transverse muscle was published previously (Kier and Curtin, 2002) but because we used a different method to make the muscle fiber bundle preparations from that of Kier and Curtin (2002), we included experiments on the arm transverse muscles to ensure consistency in the data we present on various squid muscles.

We found significant diversity in the length–force relationship across obliquely striated muscles, and observed superelongation only in the tentacle longitudinal fibers. We measured significant variation in fiber ultrastructure between the arm and tentacle that is consistent with differences in myofilament stagger, which could account for changes in the shape of the length–force relationship (Olszewski-Jubelirer, 2015; Taylor-Burt et al., 2018).

MATERIALS AND METHODS

Experimental animals

We captured sexually mature inshore longfin squid, *Doryteuthis pealeii* (Lesueur 1821), at night from lighted piers and docks in South Bristol and Boothbay Harbor, ME, USA, during the summer months (2017 to 2021) using squid jigs and cast nets (Calusa Trading Company, Fort Myers, FL, USA). Use of a green LED underwater light array (Green Blob Outdoors LLC, Taylor, TX, USA) improved our capture success rate.

Soon after capture, the animals were transported back to the Darling Marine Center (Walpole, ME, USA) in 19-liter buckets filled with seawater and then housed in a circular fiberglass tank (1.6 m diameter, 0.75 m depth). The tank was supplied with flow-through seawater drawn from the Damariscotta River with a salinity of 32 psu and a temperature that varied from 12 to 16°C but averaged 15°C. Animals were rarely housed for more than a few days prior to experimentation. Squid were fed small minnows (e.g. *Fundulus heteroclitus*, *Menidia menidia*, *Clupea harengus*).

Although not currently covered by Franklin & Marshall College, University of North Carolina Chapel Hill, or University of Maine Institutional Animal Care and Use Committee (IACUC) or institutional policies, the experiments described here largely comply with the guidelines outlined by the Association for Assessment and Accreditation of Laboratory Animal Care International (AAALAC International) regarding the capture, transport, housing, care and anesthesia of squid.

Tissue preparation

All of the 'muscles' we studied are, in fact, muscular hydrostatic organs (Kier and Smith, 1985) composed of connective tissues plus groups of obliquely striated muscle fibers oriented in two or more mutually perpendicular directions. Thus, we obtained thin sheets of muscle tissue from five muscular hydrostatic organs (arms, fins, funnel retractor, head retractor and tentacles; Fig. 2) that contained intact bundles of the fibers of interest along with fragments of connective tissue and muscle fibers whose long axes were perpendicular to the section plane of the sheet or to the fibers of interest (techniques described below). See Kier and Thompson (2003) for morphological descriptions of the five muscular hydrostatic organs.

Squid were anesthetized in cold (3–4°C) seawater for 15 min prior to being euthanized by decapitation. We focused on only one group of muscle fibers in each specimen. The target muscular hydrostatic organ (arm, fin, funnel retractor, head retractor or tentacle) was carefully dissected from the body using broken high-carbon steel razor blades and transferred immediately to a chilled (4°C) squid saline solution containing (in mmol l^{-1}): NaCl 470, KCl 10, $CaCl_2{\cdot}2H_2O$ 10, $MgCl_2{\cdot}6H_2O$ 50, glucose 20 and Hepes 10, adjusted to pH 7.8 with 2 mol l^{-1} NaOH (Milligan et al., 1997). The probability of a successful experiment was highest if the muscle tissue was kept cold and if the squid saline solution was changed at regular intervals.

A smaller segment of the organ was then dissected and glued with *n*-butyl cyanoacrylate (Vetbond, 3M, St Paul, MN, USA) to the temperature-controlled stage of a vibratome as described below.

The tentacle stalk was pinned to a Petri dish lined with Sylgard (WPI, Inc., Sarasota, FL, USA), skinned with fine forceps, and then 1 cm lengths were excised (orange dotted lines in Fig. 2A) and glued to the vibratome stage. The skinning was necessary to prevent mucus secreted by glands in the skin from reducing the strength of the adhesion between the glue and the tentacle stalk. The stalk segment was glued to the stage with its broader and relatively flat side down to allow cutting of sections parallel to the long axes (orange double-headed arrow in Fig. 2A) of the longitudinal fibers. See the dashed line in Fig. 2C for the approximate position of the section plane. Note that the surface of the tentacle stalk to the right of the dashed line in Fig. 2C was glued to the vibratome stage.

Arm pair no. 3 was excised, the suckers were removed and cross-sections (red dotted lines in Fig. 2A) approximately 3–4 mm in thickness were cut. Because the arms taper, the larger of the two cut surfaces was glued to the vibratome stage for stronger attachment, and cross-sections that contained intact bundles of the transverse muscle fibers were cut (see red double-headed arrow in Fig. 2A for long axes of transverse fibers).

The fin was skinned immediately after decapitation and a 1 cm wide section (black dotted lines in Fig. 2A) was excised and glued ventral-side down to the vibratome stage to permit the cutting of sheets of fin tissue parallel to the long axes (black double-headed arrow in Fig. 2A) of the transverse fibers. The tissue sheets were examined carefully and only those that lacked the dorsal, median or ventral fascia were used to make muscle preparations.

The middle third of the funnel retractor and head retractor organ was sliced transverse to its long axis into a 1 cm long segment, and then the segment was glued to the stage with its long edge down. This allowed sections parallel to the long axes (arrows in Fig. 2B) of the longitudinal fibers to be cut.

Journal of Experimental Biology (2023) 226, jeb244949. doi:10.1242/jeb.244949

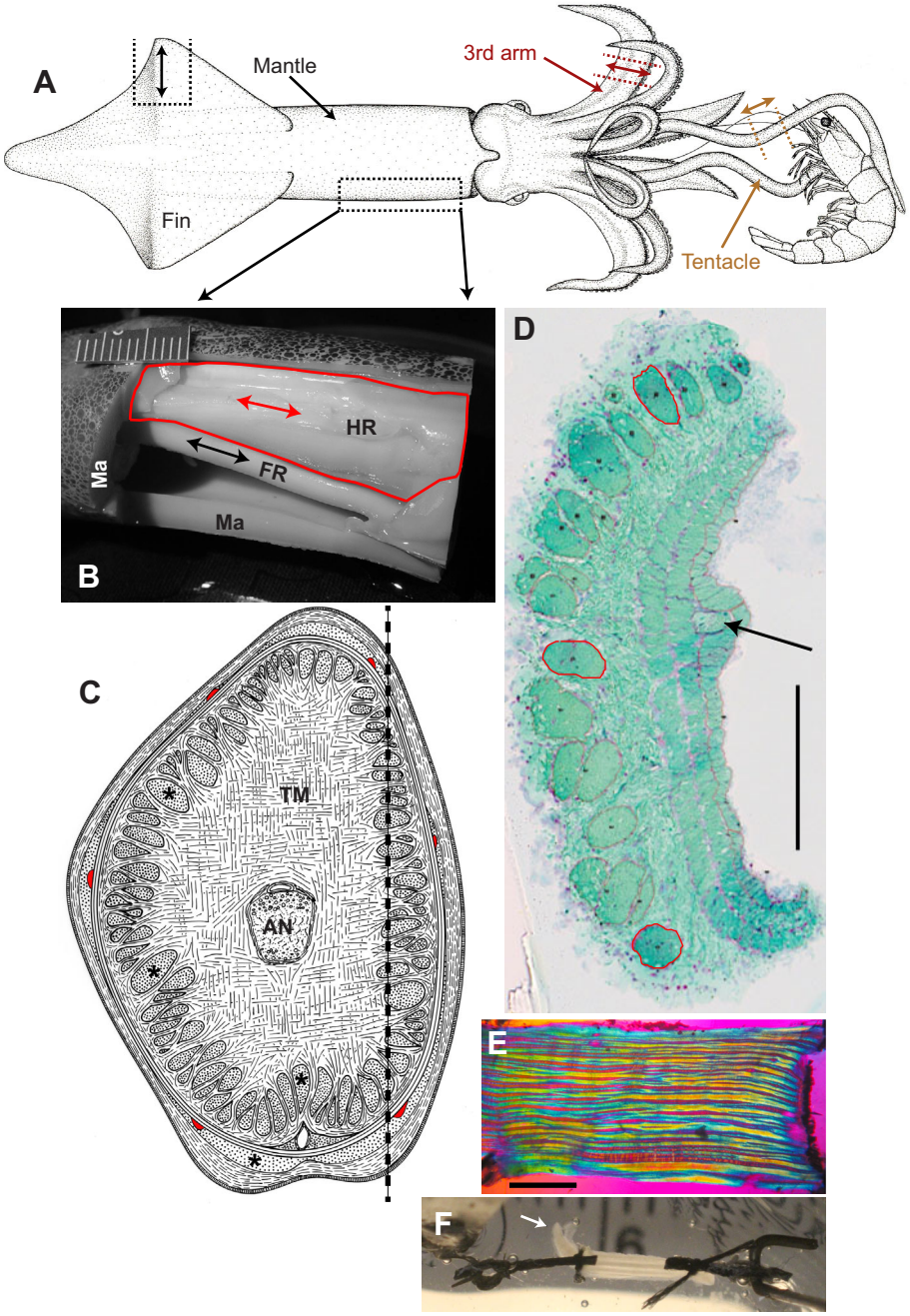

Fig. 2. Squid muscle anatomy and muscle preparations. (A) Dorsal view of a squid illustrating the fins, mantle, arms and tentacles. Doubled-headed arrows indicate the long axes of the muscle fibers investigated. Dotted lines on arm, fin and tentacle indicate the tissue segments that were excised and glued to the vibratome stage. Adapted from Kier (1985). (B) Lateral view of the right side of the body of a formalin-fixed adult *Doryteuthis pealeii* from the region indicated by the dashed lines in A. The mantle (Ma) has been cut away to reveal the positions of the head retractor (HR) and funnel retractor (FR) muscles. Double-headed arrows show the long axes of the longitudinal muscle fibers. Ruler shows millimeters. (C) Schematic diagram of a cross-section of the tentacle, illustrating the longitudinal fiber bundles, a few of which are indicated by asterisks. The dashed line shows the approximate section plane of the vibratome. The six intramuscular nerve cords are outlined in red. AN, axial nerve cord; TM, transverse muscle fibers. Adapted from Kier (1991). (D) Histological section of tentacle longitudinal muscle preparation stained with picrosirius. Three of the longitudinal muscle bundles are outlined in red. Arrow indicates an intramuscular nerve cord. Scale bar: 200 μm. (E) Vibratome-sectioned sheet of tentacle tissue viewed through crossed polarizing filters and a first-order red filter. The bundles of longitudinal fibers have their long axes oriented left to right, and are yellow/gold in color. Transverse muscle fibers (darker colors) are oriented with their long axes extending out of the plane of the image toward the viewer. Scale bar: 2 mm. (F) Tentacle longitudinal muscle preparation tied to two transducer loops and attached to the hooks of a force transducer and length controller. White arrow indicates the free end of the preparation that was dabbed with Vetbond. See Materials and Methods for details. Ruler shows millimeters.

Once the tissues were glued in the appropriate orientation, the trough containing the temperature-controlled stage of the vibratome was filled with the chilled squid saline and maintained at 4°C. Generally, the blade was positioned so that the first pass would barely graze the top of the tissue segment. In subsequent passes of the blade, sheets of tissue were cut at a thickness of 300 μm. The fin and arm tissues were much stiffer than tissue from the other muscular organs, and cutting several good sheets of uniform thickness was comparatively easy. The other tissues, however, were less stiff and uniformly thick tissue sheets were typically obtained only once the vibratome blade was positioned within 1 mm of the surface of the stage. The tentacle, in particular, was so deformable that cutting uniformly thick tissue sheets was often possible only when the vibratome blade was positioned 700–800 μm above the surface of the stage. For the less stiff tissues, adjusting the vibration amplitude of the vibratome to maximum and the advance speed to its lowest setting was helpful. Occasionally pausing the advance of the blade for a second or two after each small advance (~1 mm) also helped to produce tissue sheets of uniform thickness.

The 300 μm thick tissue sheets were then transferred to a Sylgard-lined Petri dish filled with fresh chilled (4°C) squid saline solution, immobilized with Number 000 stainless steel insect pins (Fine Science Tools, Foster City, CA, USA) inserted into the margins of the sheet, and then viewed under polarized light on a dissecting microscope. Because all of the muscle fibers we studied were derived from muscular hydrostatic organs, each sheet contained intact bundles of the fibers of interest along with fragments of connective tissue and muscle fibers (see Fig. 2D,E) whose long axes were perpendicular to the section plane of the vibratome knife or the longitudinal axis of the fibers of interest. Polarized light helped to

identify the regions of each tissue sheet that contained the majority of the fibers of interest (see Fig. 2E). We then used broken high-carbon steel blades to excise small muscle preparations that were 1–2 mm in width and 5–8 mm in length.

Each end of the tissue preparation was tied to a 'transducer loop'. The transducer loops allowed us to attach the preparations to force transducers and length controllers, and were composed of short (5–8 mm), straight lengths of 3/0 surgical silk that we modified to include a loop at one end (see left side of Fig. 2F). We used a piece of 6/0 surgical silk to tie each end of the preparation snugly to the straight portion of the 3/0 silk, with the result that a finished preparation was composed of a transducer loop at each end with the muscle preparation suspended collinearly between them (Fig. 2F). A small piece of tissue at each end projected just past the 6/0 silk that knotted the preparation to the 3/0 silk. These free ends were carefully blotted dry with small pieces of lint-free paper (Kimwipe, Kimberly-Clark, Inc., Roswell, GA, USA) and then dabbed with a tiny droplet of Vetbond to create a rigid region that could not easily slide past the knotted 6/0 surgical silk as the muscle preparation experienced increasing tensile loads. Moreover, it allowed us to tie the muscle preparation to the transducer loops snugly but without applying too much force with the 6/0 silk, to avoid severing the preparation at the knots. See Supplementary Materials and Methods (Fig. S5) for more details on transducer loop construction and the tissue attachment process.

Mechanical testing apparatus

The muscle preparations were transferred to a temperature-controlled muscle bath, superfused with the squid saline solution, and maintained at a temperature of 15°C. The transducer loops of some preparations were attached at one end to an Aurora Scientific (ASI, Inc., Aurora, ON, Canada) 300B muscle lever and at the other end to an ASI 404B force transducer. For this apparatus, stimulation parameters, servomotor lever position and force were controlled and recorded using ASI 610A Dynamic Muscle Control v5.50 software and a National Instruments (Austin, TX, USA) 16-bit A/D card. The transducer loops of other preparations were attached at one end to an ASI 322C length controller and at the other end to an ASI 400A force transducer. For this second apparatus, the ASI 600A Digital Controller and software (ASI 600a, version 3.0) paired with a National Instruments 16-bit A/D card controlled the experiments and recorded data. Both muscle mechanics rigs were used for measuring the length–force and stimulus frequency–force relationships of preparations from all 5 muscle groups. The first apparatus (i.e. the one equipped with the ASI 300B lever system) alone was used to measure the force–velocity relationship of the tentacle longitudinal muscles. For both apparatus, muscle preparation data were recorded at between 5000 and 10,000 samples s^{-1}.

Length–force and stimulus frequency–force relationships

Once the preparation was attached to the transducers/length controllers, it was lengthened until the slack was barely removed. The stimulation current that elicited the highest force was then determined using a twitch-style stimulus (0.002 s pulse width, 2 min between stimulations) delivered via platinum foil electrodes that were of sufficient size to cover the preparation. For some of the tentacle longitudinal muscle preparations, brief tetanic stimulation (0.002 s pulse width, 50 Hz, 0.1 s duration, 5 min between stimulations) was required for determining the appropriate stimulus current because the twitch-style stimulations resulted in inconsistent force outputs. Preliminary experiments for each muscle focused on using brief tetanic stimulation to find L_0 and then determining the stimulus frequency–force relationship with the preparation held at that length. Data from these preliminary experiments were used to establish the optimal stimulus frequency for the experiments on each fiber type and were not included in subsequent analyses.

The length–force relationship for each muscle was measured using the stimulation frequency that elicited the maximum tetanic isometric force. We began the length–force experiments by adjusting the preparation to the shortest length possible without sagging. Following isometric tetanic stimulation, the preparation was lengthened by 3–4% of its initial length, and then stimulated again after a 5 min rest period. Periodically and also at the end of the length–force experiment, the preparation was returned to L_0 and stimulated again. The experiment was terminated and the data discarded if the preparation was unable to produce at least 90% of its maximum isometric tetanic force (P_0).

For ease of comparison, forces and lengths were normalized. Relative forces (P/P_0) were found by dividing force by P_0, and relative lengths (L/L_0) were calculated by dividing length by L_0, the preparation length at which P_0 was produced.

The average length–force relationship for a given muscle was determined by binning the data by relative length in increments of $0.05L_0$ and finding the average relative force and length of each bin. If an individual had more than one measurement in a given bin, these data were averaged first before averaging across specimens, ensuring that an individual contributed to each bin only once.

The breadth of the ascending limb of the length–force curves at $0.6P_0$ was measured as the difference between L_0 and the length at $0.6P_0$. As measurements were not taken at exactly $0.6P_0$ in most cases, the length at $0.6P_0$ was calculated by fitting a line to the linear portion of the ascending limb ($<0.8P_0$). For this analysis, we excluded any experiments with fewer than three measurements below $0.8P_0$, exceptionally non-linear ascending limbs, and those that did not include measurements below $0.6P_0$. The differences between breadth of the length–force curves at $0.6P_0$ among muscle preparations were analyzed with ANOVA and *post hoc* pairwise comparisons using Tukey's correction for multiple comparisons.

The stimulus frequency–force relationship was explored in greater depth in the tentacle longitudinal preparations (n=7). Following a successful length–force experiment, the preparation length was adjusted to L_0 and then it was stimulated isometrically at a variety of stimulus frequencies between 1 and 300 Hz. Relative forces were compared by performing paired t-tests between stimulus frequencies.

Force–velocity relationship

The force–velocity relationship was measured for 10 of the tentacle longitudinal muscle preparations following methods outlined in Kier and Curtin (2002). Briefly, L_0 was determined for each preparation following the procedures outlined above. The preparation was held at L_0 and then stimulated tetanically (0.002 s pulses, 150 Hz, 0.1 s duration, 5 min rest period between stimulations) with the 300B servomotor in its force-clamp mode. The velocity of shortening was measured from the recordings of servomotor arm position. Isometric control stimulations were used after every 5th isotonic contraction to monitor force decline. The experiment was terminated and the data discarded if force declined by more than 10% of P_0.

A form of Hill's equation (Hill, 1938) was fitted to the force–velocity data for each preparation: $V=V_{max}P^*(P^*-P_S)/(GP_S+1)$, where V is the shortening velocity (in L_0 s^{-1}) and P_S is the force

during shortening divided by maximum isometric force. The adjustable constants are V_{max} (the intercept on the velocity axis), P^* (the intercept on the force axis) and G (the constant expressing curvature) (Kier and Curtin, 2002).

Physiological cross-section

After a successful experiment, the muscle preparation was pinned out at L_0 in a Sylgard-lined dish and fixed for 24–48 h in a solution of 3.75% formaldehyde in squid saline. Following fixation, the preparations were stored in 70% ethanol for several weeks.

Short (2–3 mm length) segments of the fixed preparations were excised from between the transducer loops (Fig. 2F), dehydrated in 95% ethanol, and then embedded in glycol methacrylate (GMA, Technovit 7100, Electron Microscopy Sciences, Hatfield, PA, USA). Sections (0.5 µm thick) transverse to the long axis of the preparation were cut with a diamond knife, mounted on slides, stained with Picrosirius (Cerri and Sasso-Cerri, 2003) and coverslipped. The aggregate cross-sectional areas of the longitudinal fiber bundles were measured from photomicrographs (Fig. 2D) using ImageJ (Schneider et al., 2012). Portions of the photomicrographs also contained the cut remnants of transverse, circular and helical muscle fibers. These were excluded from the physiological cross-sectional area calculations because they did not contribute to active force.

Transmission electron microscopy

The L_0 of fiber bundle preparations of the transverse muscle mass of the arms and the longitudinal muscle of the tentacles of *D. pealeii* was determined with isometric tests as described above. The preparations were then pinned at L_0 in a Sylgard-lined dish and fixed in 3.0% glutaraldehyde, 0.065 mol l^{-1} phosphate buffer, 0.5% tannic acid and 6% sucrose for 6–8 h at 4°C. Following fixation, the preparations were stored at 4°C in 1.0% glutaraldehyde in 0.065 mol l^{-1} phosphate buffer. A 2–3 mm portion of the preparation was cut from a point approximately midway between the suture knots securing the preparation to the loops (Fig. 2F), rinsed for 1 h in 0.065 mol l^{-1} phosphate buffer and post-fixed for 40 min at 4°C in a 1:1 mixture of 2% osmium tetroxide and 2% potassium ferrocyanide. The tissue blocks were rinsed in chilled 0.065 mol l^{-1} cacodylate buffer for 15 min and then dehydrated and cleared in a graded series of acetone. Acetone was used instead of propylene oxide and ethanol to minimize dimensional changes from dehydration and clearing (Page and Huxley, 1963). The tissue blocks were embedded in epoxy resin (EMbed 812, Electron Microscopy Sciences). The blocks were screened by examining 0.5–1.0 µm sections in the light microscope followed by trimming for ultramicrotomy of the area of interest. Sections of silver interference color were mounted on copper grids and stained with UranyLess (Electron Microscopy Sciences) and Reynolds lead citrate (Reynolds, 1963) and photographed on a Phillips Tecnai 12 transmission electron microscope. Both transverse and longitudinal sections of each fiber type were obtained and examined.

A preliminary assessment of potential differences in the stagger angle at L_0 between the arm transverse muscle and the tentacle longitudinal muscle was conducted on transverse sections of each muscle fiber type. Assuming similar myofilament lengths and a similar arrangement of the myofilament array, the spacing between adjacent Z-areas observed in transverse section is predicted to be smaller at lower stagger angles (see Discussion). This spacing was assessed by measuring the distance between the aligned arrays of dense bodies and sarcoplasmic reticulum that are located between the trapezoid-shaped groups of thick filaments (see Fig. 3A,B). Measurements for this analysis were made for muscle preparations from three individuals per muscle type (tentacle longitudinal and arm transverse), five images from each individual, and 7–10 measurements per image. The final dataset included measurements from 5–10 different fibers per individual and a total of n=123 measurements for the arm transverse fibers and n=165 measurements for the tentacle longitudinal fibers. Given that these are not all independent measurements (multiple measurements per image, multiple images per individual), we compared the two muscle types with a mixed effects linear model using the lmerTest package (Kuznetsova et al., 2017) in R (v.4.1.3). The model included one fixed effect ('muscle' indicating whether a sample was an arm transverse or tentacle longitudinal fiber) and two random effects: (1) 'individual' indicating from which experimental animal the sample was taken and (2) 'image' nested within individual, indicating from which of an individual's images a given measurement was made. The R syntax for this model was: spacing~muscle+(1|individual)+(1|individual:image).

RESULTS

Transmission electron microscopy of tentacle longitudinal muscle

A detailed description of the ultrastructure of the fibers of the transverse muscle mass of the arms (Fig. 3A,C) has been published previously (Kier, 1985) so the focus here was on the ultrastructure of the fibers of the longitudinal muscle of the tentacles (Fig. 3B,D). The fusiform fibers are circular to polygonal in cross-sectional shape with a mean±s.d. diameter of 3.7±0.6 µm (n=38). The myofilaments surround a central core that extends longitudinally in the fiber and includes mitochondria and the single nucleus of the fiber (Fig. 3). The fibers are thus classified as regular obliquely striated fibers (irregular obliquely striated fibers lack the central core of mitochondria) (Millman, 1967).

Tubules of the sarcoplasmic reticulum are present in the subsarcolemmal cytoplasm. The outer portion of their membranes is aligned in parallel with the sarcolemma, forming peripheral couplings with the sarcolemma (Fig. 3) (Nunzi and Franzini-Armstrong, 1981; Rosenbluth et al., 2010). As in other cephalopod obliquely striated muscles studied previously, the cells lack invaginated tubules and excitation–contraction coupling likely involves transmission of excitation from the sarcolemma directly to the sarcoplasmic reticulum (Gilly et al., 2020; Nesher et al., 2019; Rokni and Hochner, 2002; Rogers et al., 1997). The sarcoplasmic reticulum is also present in an intramyoplasmic zone (Nunzi and Franzini-Armstrong, 1981; Rosenbluth et al., 2010) in the plane of the Z-elements (Fig. 3). The Z-elements, which anchor the thin myofilaments, consist of irregularly spaced dense bodies (Fig. 3). When viewed in transverse section (Fig. 3A,B), the tubules of the sarcoplasmic reticulum and the dense bodies divide each fiber cross-section into a series of trapezoid-shaped areas of myofilaments. In longitudinal sections (Fig. 3C,D), it is apparent that the alignment of dense bodies and the associated intramyoplasmic sarcoplasmic reticulum are oriented at a small angle, termed the stagger angle (SA), to the longitudinal axis of the muscle fiber.

The spacing between adjacent Z-areas measured from micrographs of transverse sections (Fig. 3A,B) differed between the tentacle longitudinal and the arm transverse fibers. A mixed effects linear model with muscle type (arm versus tentacle) as a fixed effect, and individual squid and image (i.e. multiple photomicrographs were taken per preparation) nested within individual as random effects, showed that the spacing for the tentacle longitudinal fibers was significantly different from the

Journal of Experimental Biology (2023) 226, jeb244949. doi:10.1242/jeb.244949

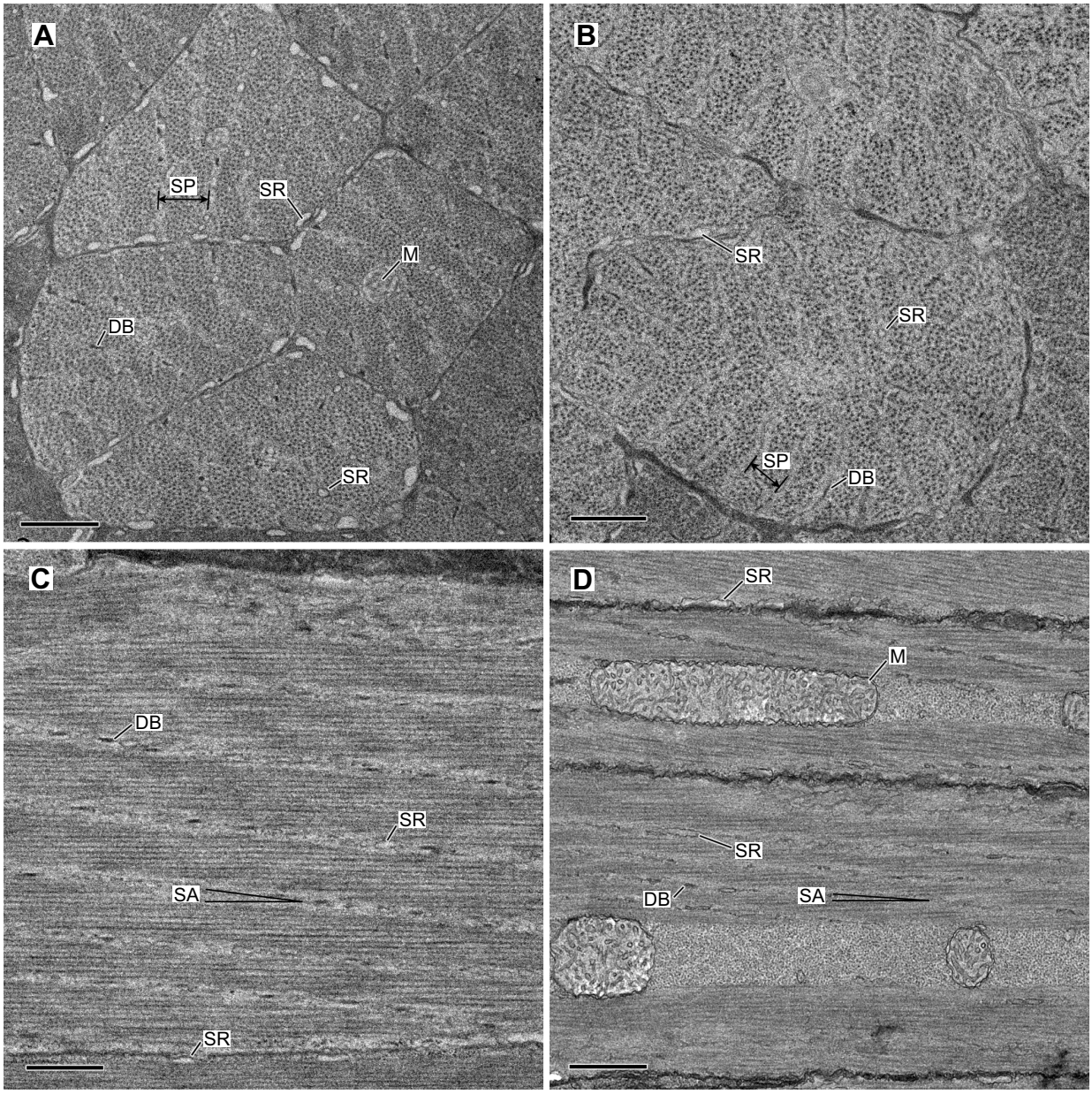

Fig. 3. Transmission electron micrographs of muscle fiber preparations of *D. pealeii* adjusted to L_0 before fixation. L_0 is the length at which maximum isometric force (P_0) is produced. (A,C) Fibers of the transverse muscle mass of the arms are shown in transverse (A) and longitudinal section (C). (B,D) Fibers of the longitudinal muscle of the tentacles are shown in transverse (B) and longitudinal (D) section. Mitochondria (M) occupy the core of the fibers. Tubules of the sarcoplasmic reticulum (SR) are located in the subsarcolemmal cytoplasm and also in an intramyoplasmic zone in the plane of the alignment of dense bodies (DB). Examples of the measurement of spacing (SP) between the adjacent alignments of dense bodies are indicated in A and B. The longitudinal axes of the fibers and the myofilaments are oriented horizontally on the page in C and D, and the dense bodies and intramyoplasmic sarcoplasmic reticulum lie in planes oriented at a small angle to the longitudinal axis of the fiber, termed the 'stagger angle' (SA). Scale bar: 1 µm in each panel.

spacing of the arm transverse fibers (t=−2.98, P=0.0427), with closer spacing for tentacle fibers (0.38±0.10 µm) than arm fibers (0.55±0.08 µm).

Relationship between stimulus frequency and force

Maximum isometric force in the tentacle longitudinal muscles was produced at stimulation frequencies between 100 and 200 Hz. Although the force produced in this range of stimulation frequencies was significantly higher than at all of the other frequencies we explored (Fig. 4; significant differences are indicated by different letters), the differences in maximum force were relatively minor (i.e. <8% of P_0) between 50 and 300 Hz.

Subsequent histological examination of the formalin-fixed and GMA-embedded tentacle muscle preparations (Fig. 2D) revealed that 4 of the 7 preparations we used for the stimulus frequency–force experiments contained one of the six intramuscular nerve cords that extend down the length of the tentacular stalk and contain both axons and nerve cell bodies (Kier, 1982). These 4 preparations produced a mean force of $0.55P_0$ with a twitch-style stimulus (i.e. a single electrical pulse) compared with a mean of $0.12P_0$ for

Journal of Experimental Biology (2023) 226, jeb244949. doi:10.1242/jeb.244949

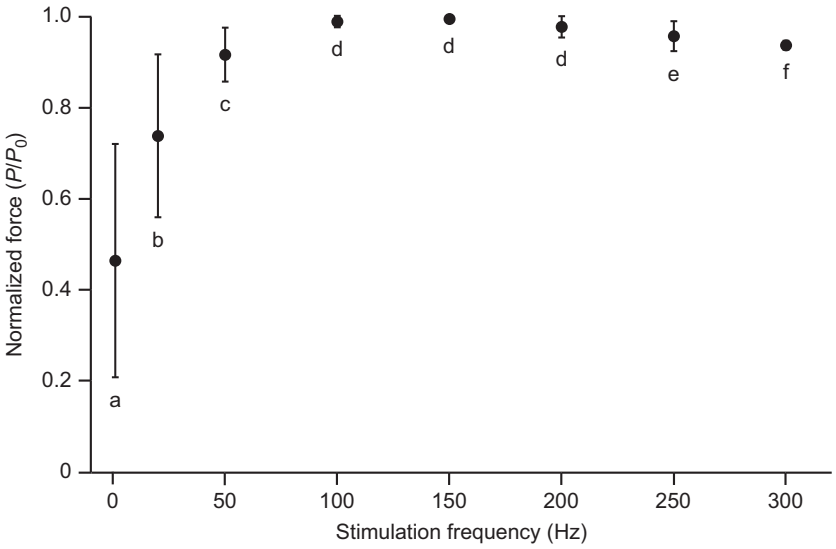

Fig. 4. Muscle force output versus stimulation frequency. Muscle force output was normalized to maximum isometric force (P_0). Different letters indicate significant differences (paired *t*-tests, $P<0.05$, $n=7$ preparations). All frequencies were significantly different from one another except for the three labeled 'd'.

preparations that lacked the nerve cord. Although we lack a detailed understanding of the role of the intramuscular nerve cords in tentacle movement, they likely function in peripheral control of the tentacle musculature. We presume that the large response to a twitch stimulus in those preparations containing portions of the axial nerve cord reflects stimulation of neurons in the axial nerve cord that innervate the longitudinal fibers, resulting in neural activation.

Maximum isometric force for the transverse muscles of the arm (150 Hz) and fin (250 Hz), and for the longitudinal fibers of the head retractor (250 Hz) and funnel retractor (250 Hz) occurred at stimulus frequencies between 150 and 250 Hz (0.002 s pulse width, 0.1 s duration). As was the case for the tentacle longitudinal muscles, there were relatively minor differences in maximum isometric force output between 50 and 300 Hz for the transverse fibers of the fin and for the longitudinal fibers of the head and funnel retractor muscles. Interestingly, all of the muscle types exhibited a slight decline in force as the stimulus frequency exceeded the value at which maximum isometric force was obtained. Thus, the common practice in muscle physiological investigations of using supramaximal stimulation frequencies is not recommended for the obliquely striated squid muscles we examined.

Maximum isometric stress of the tentacle longitudinal fibers

The tentacle longitudinal muscles produced a maximum isometric stress of 315±78 kPa (range: 233–461 kPa; $n=13$) in response to a 150 Hz stimulus with a 0.1 s duration. There was no discernible effect of the presence of the intramuscular nerve cord on the maximum isometric stress produced in response to a 150 Hz stimulus (independent samples *t*-test, $t=1.8$, $P=0.32$; $n=8$ with cord and $n=5$ without cord).

Force–velocity relationship of the tentacle longitudinal fibers

The force–velocity relationship for 10 tentacle longitudinal muscle preparations is depicted in Fig. 5. The data points for one curve are illustrated (see Fig. S1 for all data). The force–velocity relationship for each muscle preparation was determined from a mean of 28 data points (range=21–39). The single hyperbolic curve fit parameters (Hill, 1938) are listed in Table 1.

The maximum unloaded shortening velocity (V_{max}) of the tentacle longitudinal muscle at 15°C was 2.97±0.55L_0 s^{-1} (range: 1.99–4.07L_0 s^{-1}; $n=10$).

Length–force relationships for squid muscles

The average length–force relationships are shown in Fig. 6 and Fig. S2. Relationships for the tentacle longitudinal, funnel retractor, head retractor and fin transverse fibers have not been published previously. The arm transverse muscle preparation curves were independently measured for the present study but were remarkably similar to the relationship published by Kier and Curtin (2002)

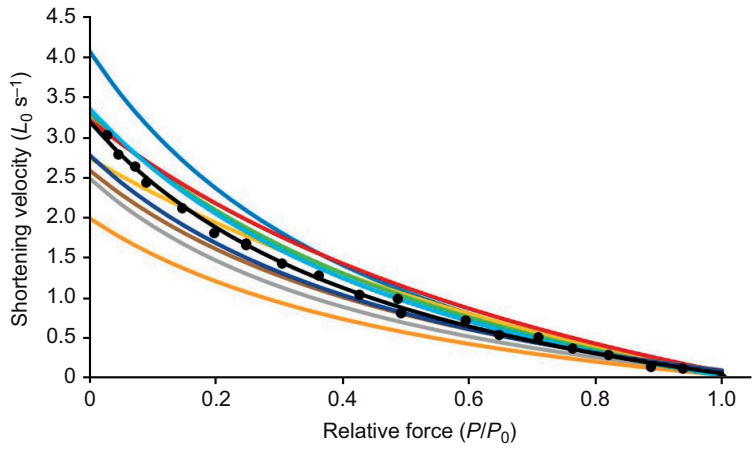

Fig. 5. Force–velocity relationship for the tentacle longitudinal muscles. Each line represents the hyperbolic fit (see Materials and Methods for details) to the data from one muscle preparation. The force–velocity data (circles) are shown for one preparation (black line). See Fig. S1 for all force–velocity data. $n=10$ preparations.

Journal of Experimental Biology (2023) 226, jeb244949. doi:10.1242/jeb.244949

Table 1. Curve fit parameters for the force–velocity experiments of 10 tentacle longitudinal muscle preparations

Preparation	P^*	V_{max}	1/G	n
1	1.1	2.77	0.568	28
2	1.02	3.35	0.625	27
3	1.1	2.59	0.621	25
4	1.05	3.21	1.00	39
5	1.03	3.29	0.735	32
6	1.05	1.99	0.588	36
7	1.02	2.74	1.43	22
8	1.08	2.48	0.515	21
9	1.06	3.19	0.524	21
10	1.05	4.07	0.503	26

The data for each preparation were fitted with a single hyperbolic curve using the following version of Hill's equation (Kier and Curtin, 2002): $V=V_{max}P^*(P^*-P_S)/(GP_S+1)$, where V is the shortening velocity (in L_0 s^{-1}, where L_0 is the muscle length at which maximum isometric force was produced) and P_S is the force during shortening divided by maximum isometric force. The adjustable constants are V_{max} (the intercept on the velocity axis), P^* (the intercept on the force axis) and G (the constant expressing curvature). n, the number of data points per muscle preparation.

(see Fig. S3 for comparison). The data for the mantle circular fibers were previously published in Thompson et al. (2014). Data were binned and averaged across individuals (see Materials and Methods for details). Because all individuals did not contribute to each bin, sample sizes are indicated for each data point in Fig. S2. The curves for the arm and fin transverse preparations did not extend as far down the ascending limb as the other preparations because these preparations tended to buckle in compression during passive shortening.

The tentacle had a broad active length–force curve with an extensive descending limb while the curves for all other preparations had very limited descending limbs (Fig. 6A; Fig. S2). Elongation of all non-tentacle muscle preparations much beyond L_0 usually resulted in damage, as evidenced by a decrease in active force when the preparation was returned to L_0. As noted in Materials and Methods, we periodically assessed the health of each preparation by measuring isometric force production at L_0 and excluded data if the preparation produced $<0.9P_0$. With this approach, the longest muscle lengths reached without damaging the preparations for the transverse fibers of the arm and the longitudinal fibers of the head retractor and funnel retractor were $1.05L_0$ (arm transverse: $1.05\pm0.02L_0$, head retractor: $1.05\pm0.03L_0$, funnel retractor: $1.05\pm0.01L_0$) and $1.04\pm0.01L_0$ for the fin transverse fibers. Length–force relationships that exhibit very limited descending limbs are similar to the circular muscle fibers of the mantle of *D. pealeii* in which the maximum extension of the preparations was $1.05L_0$ (Thompson et al., 2014). The longitudinal fibers of the tentacle, in contrast, exhibited a maximum extension of $1.23\pm0.13L_0$.

Because the descending limb was largely absent for all preparations except the tentacle, comparisons focused on the ascending limb. Linear relationships were found for the ascending limb ($R^2>0.91$) in order to calculate the length at $0.6P_0$ and the width of the ascending limb (i.e. the difference between L_0 and the length at $0.6P_0$) by individual (see Materials and Methods for details). The dataset of ascending limb widths did not violate the assumptions of normality (Shapiro test, $P=0.2384$) or of the homogeneity of variance (Levene's test, $P=0.6429$). Muscle preparation had a significant effect on the breadth of the ascending limb (ANOVA, $F_{4,34}=54.115$, $P<0.001$). *Post hoc* tests showed the width of the ascending limb of the tentacle at $0.6P_0$ ($n=12$, $0.43\pm0.04L_0$) was significantly different ($P<0.001$) from that of all other muscle preparations (arm transverse: $n=4$, 0.29

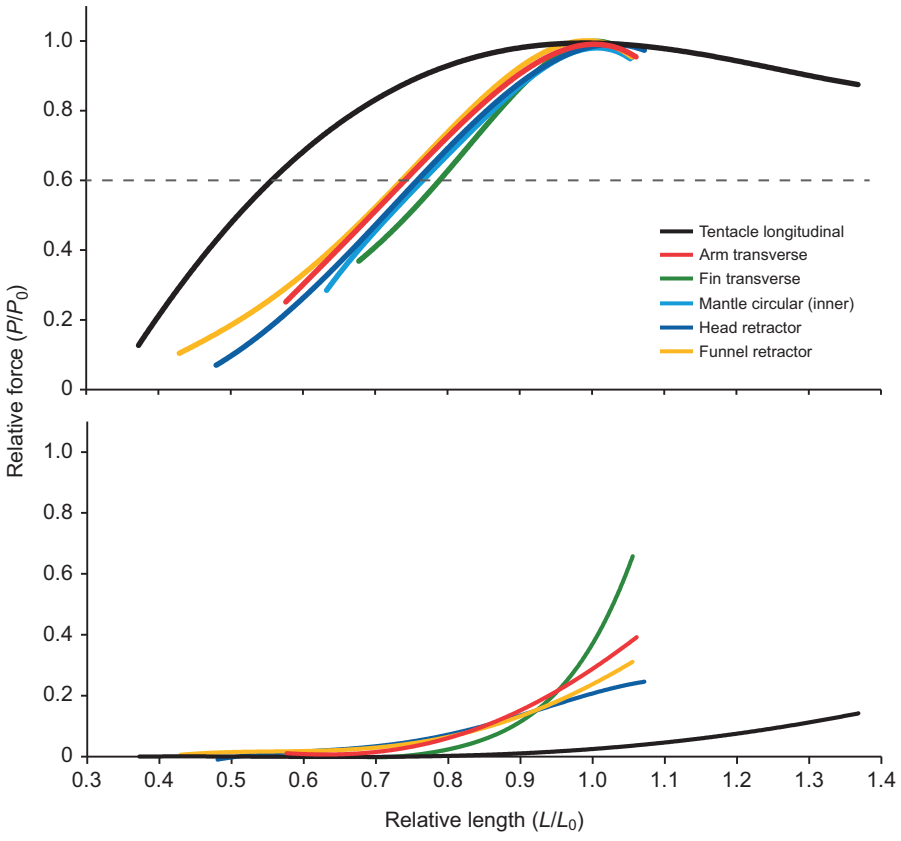

Fig. 6. Active and passive length–force relationships for squid muscles. (A) The active length–force relationship for the tentacle ($n=15$) was broad, producing 90% of peak force over a strain of $0.54L_0$. All other muscle preparations (arm transverse $n=6$, fin transverse $n=15$, head retractor $n=9$, funnel retractor $n=6$, and mantle circular: Thompson et al., 2014) exhibited narrower length–force relationships with little descending limb. At $0.6P_0$ (horizontal line), the difference between L_0 and the ascending limb was significantly greater for the tentacle than for all other muscles (ANOVA: $P<0.001$; *post hoc* pairwise comparisons using Tukey's correction for multiple comparisons: $P<0.001$). Although the head retractor, funnel retractor and arm transverse length–force relationships were not different ($P>0.05$), the fin transverse length–force relationship was narrower than that for the arm transverse ($P=0.004$) and funnel retractor ($P=0.012$). (B) The passive force increased gradually only at very long lengths for tentacle longitudinal preparations, while the other muscle preparations were stiffer, with passive forces rising quickly at shorter lengths. A and B share the same *x*-axis. Curves are 4th order polynomial fits to averaged length–force data. Data points and error bars are not included here for clarity but can be found in Fig. S2. Note that not every animal contributed to every bin; sample sizes by data point are reported in Fig. S2.

±0.03L_0; head retractor: n=6, 0.24±0.06L_0; fin transverse: n=11, 0.20±0.04L_0, funnel retractor: n=6, 0.27±0.03L_0). The arm, funnel retractor and head retractor were not different from one another (P>0.05), and the head retractor was not different from the fin transverse (P>0.05). However, the breadth of the ascending limb for the fin transverse preparations was significantly lower than that for the arm transverse (P=0.004) and the funnel retractor (P=0.012). These data demonstrate that obliquely striated muscle length–force relationships vary significantly even within the same species.

The passive force increased gradually only at long muscle lengths for tentacle longitudinal preparations, while the other muscle preparations were stiffer, with passive forces rising rapidly at shorter lengths (Fig. 6B). For example, passive force in the arm, fin and funnel retractor muscle preparations was 0.2P_0 or higher at L_0, whereas the mean passive force did not reach 0.2P_0, even at the longest tentacle preparation lengths (Fig. 6B). The relatively low passive force of the longitudinal tentacle fibers is consistent with their extensive *in vivo* operating range (i.e. whole-tentacle elongation strains ≥0.8; Kier, 1982; Kier and Van Leeuwen, 1997).

DISCUSSION

The principal findings of our investigation of five squid muscles are as follows: (1) the tentacle longitudinal fibers are obliquely striated and their ultrastructure closely resembles that of other obliquely striated muscles in cephalopods, (2) the stimulus frequency–force and force–velocity relationships of the tentacle longitudinal fibers are generally similar to those of other obliquely striated muscles in *D. pealeii* but (3) the length–force relationships vary significantly and, in particular, (4) only the tentacle longitudinal fibers exhibit superelongation.

Tentacle longitudinal fibers are obliquely striated

The ultrastructural analysis confirmed that the longitudinal tentacle fibers are obliquely striated, similar to most cephalopod muscle examined previously (Amsellem and Nicaise, 1980; Bone et al., 1995; Chantler, 1983; Cloney and Brocco, 1983; Hanson and Lowy, 1960; Kier, 1989; 1996; 2016; Kier and Curtin, 2002; Shaffer and Kier, 2016; Nicaise and Amsellem, 1983; Rosenbluth et al., 2010), including the arms of *D. pealeii* (Kier, 1985).

The ultrastructural analysis also provided confirmation of the effectiveness of our procedures for maintaining the viability of the muscle fiber preparations during measurement of their contractile properties. It is typical when preparing tissues for electron microscopy to begin fixation as soon as possible following death with the goal of avoiding autolytic changes. The procedures involved in making the fiber bundle preparations and then determining L_0 require several hours. The micrographs shown in Fig. 3 were of preparations that were fixed 3.5–4 h after the death of the organisms, yet the ultrastructure appears quite well preserved.

Stimulus frequency–force and force–velocity relationships

The five *D. pealeii* muscles that we investigated produced maximum isometric force at similar stimulus frequencies, which suggests that they possess similar excitation–contraction coupling mechanisms. The maximum isometric stress of the tentacle longitudinal fibers (315±78 kPa) was approximately two-thirds of that produced by the arm transverse fibers (468±91 kPa, 160 Hz, 0.2 s duration; Kier and Curtin, 2002). Because thick filament length is proportional to force output (Josephson, 1975), it is possible that the thick filaments of the arm transverse fibers may be longer than those of the tentacle longitudinal fibers. Measurement of thick filament length will require a more extensive ultrastructural analysis than was possible here. The peak isometric stress of the tentacle longitudinal fibers was, however, similar to that of the superficial mitochondria-rich mantle circular fibers (335±35 kPa, 150 Hz, 0.2 s duration; Thompson et al., 2008) and the longitudinal fibers of the funnel retractor (270±20 kPa, 150 Hz, 0.2 s duration; Rosenbluth et al., 2010). We did not investigate the isometric stress produced under longer stimulus durations. The mean we report is likely an underestimate of the maximum possible isometric stress given that force continued to rise and never reached a plateau either during or immediately after the stimulus.

The V_{max} of the tentacle longitudinal fibers (2.97±0.55L_0 s^{-1}) was double that of the arm transverse fibers (1.47±0.22L_0 s^{-1}, 19°C; Kier and Curtin, 2002) but was comparable to that of longitudinal fibers of the funnel retractor (2.15±0.26L_0 s^{-1}, 17°C; Rosenbluth et al., 2010) and the superficial mitochondria-rich circular fibers of the mantle (2.4±0.76L_0 s^{-1}, 20°C; Thompson et al., 2008).

Length–force relationships vary among *D. pealeii* muscles

The tentacle longitudinal fibers produced high forces over an exceptional range of lengths (Fig. 6; Fig. S2). The '90% range' (Lowy and Mulvany, 1973) is defined as the width of the active length–force curve at 0.9P_0, and is a measure of plateau breadth. The 90% range for the tentacle (0.54L_0 for the average relationship for the tentacle; Fig. 6) was 2–3 times greater than the 90% range typically found for cross-striated muscles. For example, the 90% range of bullfrog plantaris (0.19L_0; Azizi and Roberts, 2010), mouse soleus (0.24L_0; Askew and Marsh, 1998), carp jaw closers (0.13L_0; Gidmark et al., 2013) and cockroach leg muscle (0.17L_0; Ahn et al., 2006) is substantially narrower than observed for the tentacle longitudinal fibers. In fact, the tentacle has a larger 90% range than even the smooth muscle taenia coli from guinea pigs (0.47L_0; Lowy and Mulvany, 1973).

We found no evidence that superelongation is a common trait among obliquely striated muscles in *D. pealeii*. Although the breadth of the length–force relationship varied among the squid muscles we examined, only one, the tentacle longitudinal muscle, demonstrated the broad length–force relationship and high degree of extensibility characteristic of superelongating muscles. Thus, superelongation seems to be more of an exception than a rule, at least within *D. pealeii*.

We found only mixed support for the prediction that the length–force relationship varies proportionately with the strain experienced by the muscle *in vivo*. The muscle fibers measured in the present study included those estimated to experience large (tentacle longitudinal; Kier, 1982; Kier and Van Leeuwen, 1997), intermediate (head retractor, mantle circular; Thompson et al., 2014, 2016) and short (funnel retractor, fin and arm transverse; Kier, 1982; Kier et al., 1989; Rosenbluth et al., 2010) excursions *in vivo*. The shape of the length–force curves observed for squid muscles may reflect their function in some cases but for others it is unclear. For example, the tentacle longitudinal fibers exhibited a broad active length–force curve and low passive forces, as we expected given the large *in vivo* strains of the tentacle stalk during the prey strike (Kier, 1982; Kier and van Leeuwen, 1997). Similarly, the fin transverse fibers likely undergo very little length change *in vivo* (Kier, 1989; Kier et al., 1989) and correspondingly have a narrow active curve and develop passive forces at short lengths. The funnel retractor, however, experiences low strains across a range of behaviors (Rosenbluth et al., 2010) yet has one of the broader non-tentacle length–force curves for *D. pealeii* (Fig. 6).

Four of the *D. pealeii* muscle preparations (transverse arm and fin fibers; longitudinal funnel retractor and head retractor fibers) could

not be stretched much longer than L_0 without either tearing or experiencing a permanent decrease in isometric force output. This *in vitro* mechanical behavior is inconsistent with superelongation. The muscular organs from which these preparations were derived all qualitatively felt stiffer and were less deformable than the tentacle stalks, when handled immediately post-mortem. It is possible that differences in connective tissue fiber quantity and arrangement (e.g. Di Clemente et al., 2021) and/or intrinsic differences in muscle fiber stiffness underlie the differences in extensibility we observed.

Regardless of the causes, the presence of such short descending limbs for the arm, fin, funnel retractor and head retractor muscles suggests that they operate predominantly along the ascending limb of the length–force curve *in vivo*. The measurement of muscle fiber strain during movement in soft-bodied invertebrates is particularly challenging given that their bodies and organs typically lack hard parts or other reference points that can be monitored during movement to reconstruct muscle strain, as for instance is done in vertebrate studies using X-ray reconstruction of moving morphology (XROMM) (Brainerd et al., 2010). Sonomicrometry can sometimes be used (see Thompson et al., 2014, for an example), if the *in vivo* and *in vitro* strains can be precisely correlated, but the documentation of the range of muscle strain during movement in soft-bodied invertebrates remains a significant gap in our understanding. Thompson et al. (2014) showed that the obliquely striated mantle circular muscles of *D. pealeii* operate primarily on the ascending limb of the length–tension curve as do other muscles, such as the cross-striated adductor muscles of the bay scallop *Argopecten irradians* (Olson and Marsh, 1993; Marsh and Olson, 1994), the wing depressor of the hawkmoth *Manduca sexta* (Tu and Daniel, 2004), the papillary muscles of mammals (Allen and Kentish, 1985; Layland et al., 1995), the atrial trabeculae of frogs (Winegrad, 1974), and human soleus muscles (Rubenson et al., 2012). Operating on the ascending limb has been suggested to allow cyclically active muscles to respond to a stretch by increasing their capacity to produce force, though at the cost of decreased work and power. In addition, operation on the ascending limb is hypothesized to provide non-neural mechanisms for regulating muscle excursion lengths during cyclical contractions (Rubenson et al., 2012; Tu and Daniel, 2004). Although it is unclear whether these hypotheses apply to the muscles we studied, the fins (Kier, 1989; Kier et al., 1989), funnel retractor (Rosenbluth et al., 2010) and head retractor (Thompson et al., 2016) are all involved in rhythmic movements during jetting and fin undulation.

Comparison of length–force relationships among cephalopods and annelids

Across taxa, obliquely striated muscles display a range of length–force relationships (Fig. 7; Fig. S4). This includes diversity in the breadth of the length–force curve within a taxon for animals with different feeding behaviors (leeches), within a species (earthworm), and even within the same muscular hydrostatic organ (octopus arm). The squid arm, fin, head retractor, funnel retractor and mantle muscle preparations all have relatively narrow length–force relationships, similar to those observed for the earthworm longitudinal and circular muscles (Hidaka et al., 1969; Tashiro and Yammamoto, 1971). Conversely, the tentacle longitudinal fibers have an exceptionally broad length–tension curve that is only narrower than that of the longitudinal body wall muscles of the blood-feeding leech, *Hirudo verbana* (Gerry and Ellerby, 2011). Thus, the diversity of length–force relationships we observed for squid muscle fibers was not an anomaly but rather seems to be a common characteristic of obliquely striated muscle.

There are several differences in the length–force relationship among cephalopod obliquely striated muscles. The arm transverse and longitudinal fibers of *O. vulgaris* have similar relatively broad ascending limbs and fairly extensive, though different, descending limbs (Fig. 7; Fig. S4; Zullo et al., 2022). The arm transverse fibers of *O. vulgaris* exhibit a broader length–force relationship than the arm transverse fibers of *D. pealeii*, perhaps reflecting the greater extensibility observed in octopus arms (Hanassy et al., 2015; Kennedy et al., 2020; Levy et al., 2015; Margheri et al., 2012; Mazzolai et al., 2013) compared with squid arms (Kier, 1982). The arm transverse fibers in octopus are responsible for elongation of the arms and support for bending (Kier and Stella, 2007) while those in the arms of squid primarily support bending with little length change (Kier, 1982). Based on measurements of *O. vulgaris* whole-arm dimensions in a relaxed state, Di Clemente et al. (2021) showed that the inherent elasticity of the arm resulted in stretching of the transverse muscle fibers and compression of the longitudinal fibers, relative to their length when removed from the arm. This means that during elongation of the arm by the transverse muscle fibers, the longitudinal muscles are initially at a short length and considerable elongation can occur before the fibers approach L_0, consistent with other obliquely striated muscles discussed above that operate primarily on the ascending limb of the length–force relationship.

Gerry and Ellerby (2011) observed an exceptionally broad length–force relationship for longitudinal body wall muscle of the leech *H. verbana* (Fig. 7; Fig. S4). In addition, they showed that the presence of serotonin (10 µmol l^{-1}) in the muscle preparation bathing solution reduced passive stress and substantially increased active stress. Interestingly, Miller (1975) reported a much narrower length–force relationship for the longitudinal body wall muscle of a different leech (*Haemopis sanguisuga*), although its ascending limb is broader than that of all of the other obliquely striated muscles except for *H. verbana* and the tentacle longitudinal fibers (Fig. 7; Fig. S4). It is unclear whether the narrower length–force relationship in *H. sanguisuga* was due to the absence of serotonin in the muscle bathing solution or to differences in feeding biology of the two leeches (i.e. *H. sanguisuga* is a predatory leech whereas *H. verbana* is a blood feeder).

It's important to note that some of the variability in the length–force relationships (Fig. 7; Fig. S4) could be due to differences in stimulation parameters. Stimulation duration and frequency are known to affect the shape of the length–force relationship (Rack and Westbury, 1969). Although all of the *D. pealeii* muscles were stimulated similarly (i.e. 0.002 s pulse width, 0.1 s duration; at the frequency that produced maximum tetanic force), the stimulation parameters varied for the obliquely striated muscles of other species. For example, the earthworm longitudinal muscle was stimulated for 0.001 s by Hidaka et al. (1969) versus 0.01 s by Tashiro and Yammamoto (1971). For the leech longitudinal body wall muscles, Miller (1975) used 0.005 s pulse widths, 50 Hz, 0.5 s duration while Gerry and Ellerby (2011) used 0.001 s pulses at 80 Hz for 0.2 s duration. Nevertheless, stimulation parameters for different muscles did not differ within species for *D. pealeii*, *Octopus vulgaris* (Zullo et al., 2022; 50 Hz for 0.1 s) or the muscles of *Pheretima communissima* studied by Hidaka et al. (1969; both stimulated for 0.001 s), and thus are not the cause for the variation observed in these examples.

Our data and the previously published work on obliquely striated muscle demonstrate that while superelongation occurs in two species, it does not appear to be a universal feature of this type of muscle. Instead, these muscles exhibit a diversity of length–force relationships, even within the same species or the same muscular

Journal of Experimental Biology (2023) 226, jeb244949. doi:10.1242/jeb.244949

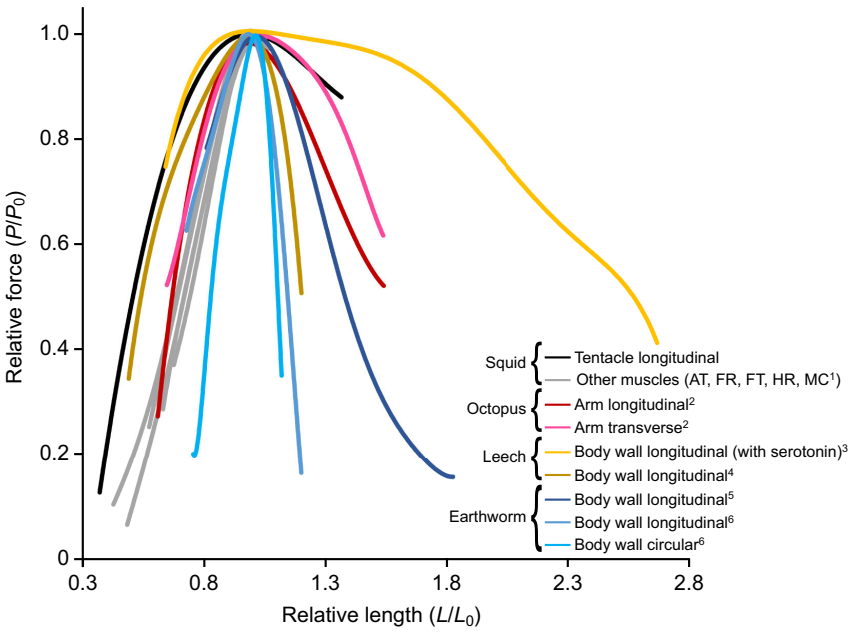

Fig. 7. Diversity of length–force relationships. Squid curves are polynomial fits for averaged data. For ease of comparison, the squid tentacle longitudinal muscle (black) is distinguished from the other squid muscles (gray: AT, arm transverse; FT, fin transverse; HR, head retractor; FR, funnel retractor; MC, mantle circular, inner, from Thompson et al., 2014). See Fig. 6 and Figs S2 and S4 for more details. Curves for other species are polynomial fits to digitized points or curves from previously published figures. Source data and species are: [1]Thompson et al. (2014), *Doryteuthis pealeii*; [2]Zullo et al. (2022), *Octopus vulgaris*; [3]Gerry and Ellerby (2011), *Hirudo verbana*; [4]Miller (1975), *Haemopis sanguisuga*; [5]Tashiro and Yamamoto (1971), *Pheretima communissima*; [6]Hidaka et al. (1969), *P. communissima*. Note that the two leech curves were measured in different species.

organ. The superelongation observed for leech longitudinal body wall muscle and tentacle longitudinal muscle may represent a specialized form of obliquely striated muscle, in contrast to the long-held assumption that superelongation drove the evolution of the oblique striation pattern. Although the current hypothesis of the mechanism of superelongation requires oblique striation in order to function, we hypothesize that superelongation was a secondary adaptation (Lanzavecchia, 1977; Lanzavecchia and Arcidiacono, 1981; Lanzavecchia and De Eguileor, 1976).

Mechanisms to alter length–force relationships in obliquely striated muscle

Oblique striation may have evolved as a structural modification that permits ‘tuning’ the length–force properties of a muscle fiber by altering the myofilament stagger angle. Olszewski-Jubelirer (2015) developed a simple, two-dimensional mathematical model that predicts that the length–force relationship of an obliquely striated muscle depends on the myofilament stagger angle at L_0 (Olszewski-Jubelirer, 2015; see Taylor-Burt et al., 2018, for details). The model takes into account the constant volume of the fiber and the stagger angle as a function of length to determine the overlap between thick and thin myofilaments, and thereby calculates the resulting stress relative to maximum overlap. Interestingly, the model predicts that, as the resting stagger angle decreases, the length–force relationship broadens.

We conducted a preliminary assessment of the model’s predictions by comparing the ultrastructure of the transverse muscle fibers of the arms and the longitudinal muscle fibers of the tentacles. As described above, the tentacle fibers have a broader length–force relationship and greater *in vivo* operating length range than the arm transverse fibers. The model thus predicts that the stagger angle of the tentacle fibers should be lower than that of the arms at L_0.

Direct measurement of stagger angle on electron micrographs of longitudinal sections of obliquely striated muscle is, however, challenging because obtaining precise longitudinal sections and verifying their orientation is difficult. In addition, the surfaces defined by the aligned Z-elements are curved helixes in cephalopod obliquely striated muscles, analogous to the shape of an Archimedes screw, so the intersection with the section plane is curved, complicating the measurement of angle.

We instead conducted a preliminary assessment of the stagger angle using electron microscopy of transverse sections of the arm transverse fibers and the tentacle longitudinal fibers, both fixed at L_0. Because the stagger angle increases as an obliquely striated fiber shortens, and decreases as it elongates, at higher stagger angles, the spacing in transverse section between the surfaces defined by the aligned Z-elements is greater than that at lower stagger angles (Fig. 1B–D). Thus, if the myofilament dimensions of two obliquely striated muscle fibers are the same, narrower transverse spacing is associated with a lower stagger angle.

We observed significantly narrower spacing between the Z-areas in transverse section in the tentacle longitudinal fibers, consistent with a lower stagger angle, as predicted by the model. Nevertheless, we regard this conclusion as preliminary until a more extensive ultrastructural analysis can be conducted, in particular to measure myofilament lengths in these two fiber types. If, for instance, the thick and thin myofilaments are longer in the arm transverse fibers, at a given stagger angle the transverse spacing would be wider than that of the tentacle fibers. Indeed, the higher peak isometric stress of the arm fibers and the higher unloading shortening velocity of the tentacle fibers that we observed could be due to longer myofilaments in the arm fibers. Thus, additional work is needed to determine the role of stagger angle in modulating the length–force properties of obliquely striated muscle.

Another mechanism for altering the length–force relationship, termed the ‘changing partners’ hypothesis, was proposed by Miller (1975) for the longitudinal body wall muscles in the leech *H. sanguisuga*. She hypothesized that the staggered myofilament array would allow thick filaments to form cross-bridges with new thin filaments (i.e. new partners) when pulled beyond overlap at progressively longer muscle lengths (see Fig. 1B–D for a schematic representation), thereby maintaining the overlap between thick and thin filaments and allowing for superelongation. Although Lanzavecchia and colleagues used mathematical modeling and ultrastructural studies to explore ‘changing partners’ in greater depth (Lanzavecchia, 1977; Lanzavecchia and Arcidiacono, 1981;

Lanzavecchia, 1985), the changing partners hypothesis remains untested.

New directions

The Biomechanics Special Issue provides an opportunity to reflect on the importance of seminal papers in the field. Publications in Journal of Experimental Biology have played a crucial role in the development of our understanding of hydrostatic skeletons and obliquely striated muscle. The journal has published key foundational papers on the role of the musculature in movement in hydrostatic skeletons (Batham and Pantin, 1950) and, of special relevance to this paper, the implications of hydrostatic skeletal support for the changes in length experienced by circular versus longitudinal muscle (Chapman, 1950), in addition to the control of extensibility by the connective tissues of the body wall (Clark and Cowey, 1958; Harris and Crofton, 1957; see Shadwick, 2008). Furthermore, many of the early papers on the physiology and mechanics of obliquely striated muscle were also published in Journal of Experimental Biology (Hidaka et al., 1969; Miller, 1975; Tashiro, 1971; Tashiro and Yamamoto, 1971). The journal continues to be a home for the ongoing work in obliquely striated muscle (e.g. Di Clemente et al., 2021; Gilly et al., 2020; Kier and Curtin, 2002; Milligan et al., 1997; Thompson et al., 2014; Zullo et al., 2022).

The Special Issue also prompts us to look forward to new directions in research on obliquely striated muscle. Compared with cross-striated muscle fibers of vertebrates and arthropods, obliquely striated muscle has received relatively little attention. We have limited understanding of the three-dimensional architecture of the myofilament array and of the implications of variation in this architecture for the contractile properties. Variation has been observed in the alignment of the dense bodies (helical versus oblique; Rosenbluth, 1968), myofilament length and thin:thick ratio (Thompson and Kier, 2006; Thompson et al., 2010), myofilament stagger (Hanson and Lowy, 1957; Millman, 1967; Rosenbluth, 1965), potential structural connections between adjacent myofilaments (Rosenbluth, 1967; 1968; 1972), and potential changes in myofilament spacing (Lanzavecchia et al., 1985). All of these likely have important implications for length–force and force–velocity properties of the muscle (e.g. Williams et al., 2013). In addition, we know little about giant muscle proteins in obliquely striated muscles, although there are several such proteins in the obliquely striated body wall muscles of *Caenorhabditis elegans* (see Hooper and Thuma, 2005, for a review), and antibody labeling revealed a large titin-like protein in squid mantle tissue (Kasamatsu et al., 2004). A titin-like giant protein extending from the Z-areas to the middle of a thick filament would not only affect the contractile properties but also have potential implications for the proposed mechanism of superelongation by ‘changing partners’ described above. Finally, evolutionary analyses of the patterns of obliquely striated muscle evolution are needed in order to provide context for functional studies of this important muscle type.

In conclusion, our findings require a re-examination of long-held ideas about the structure–function relationships in muscles. If not for superelongation, what factors favored the evolution of oblique striation multiple times? How do the functions of obliquely striated muscle differ from those of other striated muscle types? What physiological mechanisms allow some muscles to superelongate but not others? Although perhaps not as familiar as vertebrate and arthropod systems, the obliquely striated muscles of soft-bodied invertebrates provide an exciting opportunity to investigate general principles of striated muscle specialization and to gain new perspectives on the biomechanics of hydrostatic skeletons.

Acknowledgements

We thank the staff at the Darling Marine Center for help with laboratory space and housing, especially Linda Healy, Dr Heather Leslie, Tim Miller, Matt Norwood and Lisa Ouellette. The experiments were conducted with the assistance of Rashi Anand, Gustavo Hernandez, Nicole Hsing-Smith and Hallie Keatley. We also thank Rashi Anand, Timmy Burt, Gustavo Hernandez, Nicole Hsing-Smith, Hallie Keatley, and Claire, Ian and Sophie Thompson for assistance with capturing and maintaining squid. Electron microscopy was performed at the University of North Carolina Hooker Imaging Core Facility, supported in part by P30 CA016086 Cancer Center Core Support Grant to the UNC Lineberger Comprehensive Cancer Center.

Competing interests

The authors declare no competing or financial interests.

Author contributions

Conceptualization: J.T.T., W.M.K.; Methodology: J.T.T., K.R.T.-B., W.M.K.; Validation: J.T.T., K.R.T.-B., W.M.K.; Formal analysis: J.T.T., K.R.T.-B., W.M.K.; Investigation: J.T.T., K.R.T.-B., W.M.K.; Writing - original draft: J.T.T., K.R.T.-B., W.M.K.; Writing - review & editing: J.T.T., K.R.T.-B., W.M.K.; Funding acquisition: J.T.T., W.M.K.

Funding

This work was supported by the National Science Foundation (IOS-1755231 to W.M.K. and IOS-1755314 to J.T.T.).

References

Ahn, A. N., Meijer, K. and Full, R. J. (2006). *In situ* muscle power differs without varying in vitro mechanical properties in two insect leg muscles innervated by the same motor neuron. *J. Exp. Biol.* **209**, 3370-3382. doi:10.1242/jeb.02392

Allen, D. G. and Kentish, J. C. J. (1985). The cellular basis of the length-tension relation in cardiac muscle. *J. Mol. Cell. Cardiol.* **17**, 821-840. doi:10.1016/S0022-2828(85)80097-3

Amsellem, J. and Nicaise, G. (1980). Ultrastructural study of muscle cells and their connection in the digestive tract of *Sepia officinalis*. *J. Submicro. Cytol.* **12**, 219-231.

Askew, G. N. and Marsh, R. L. (1998). Optimal shortening velocity (V/V_{max}) of skeletal muscle during cyclical contractions: length-force effects and velocity-dependent activation and deactivation. *J. Exp. Biol.* **201**, 1527-1540. doi:10.1242/jeb.201.10.1527

Azizi, E. and Roberts, T. J. (2010). Muscle performance during frog jumping: influence of elasticity on muscle operating lengths. *Proc. R. Soc. B Biol. Sci.* **277**, 1523-1530. doi:10.1098/rspb.2009.2051

Azizi, E., Brainerd, E. L. and Roberts, T. J. (2008). Variable gearing in pennate muscles. *Proc. Nat. Acad. Sci. USA* **105**, 1745-1750. doi:10.1073/pnas.0709212105

Batham, E. J. and Pantin, C. F. A. (1950). Muscular and hydrostatic action in the sea-anemone *Metridium senile*. *J. Exp. Biol.* **27**, 264-289. doi:10.1242/jeb.27.3.264

Biewener, A. A. and Patek, S. N. (2018). *Animal Locomotion,* 2nd edn. Oxford: Oxford University Press.

Bone, Q. and Ryan, K. P. (1974). On the structure and innervation of the muscle bands of *Dolium* (Tunicata: Cyclomyaria). *Proc. R. Soc. Lond. B Biol. Sci.* **187**, 315-327. doi:10.1098/rspb.1974.0077

Bone, Q., Brown, E. R. and Usher, M. (1995). The structure and physiology of cephalopod muscle fibres. In *Cephalopod Neurobiology: Neuroscience Studies In Squid, Octopus and Cuttlefish* (ed. N. J. Abbott), pp. 301-329. Oxford University Press.

Bouligard, Y. (1966). La disposition des myofilaments chez une annélide polychète. *J. Microscopie.* **5**, 305-322.

Brainerd, E. L., Baier, D. B., Gatesy, S. M., Hedrick, T. L., Metzger, K. A., Gilbert, S. L. and Crisco, J. J. (2010). X-ray reconstruction of moving morphology (XROMM): precision, accuracy and applications in comparative biomechanics research. *J. Exp. Zool.* **313A**, 262-279. doi:10.1002/jez.589

Burkholder, T. J. and Lieber, R. L. (2001). Sarcomere length operating range of vertebrate muscles during movement. *J. Exp. Biol.* **204**, 1529-1536. doi:10.1242/jeb.204.9.1529

Carnevali, M. D. C., Saita, A. and Fedrigo, A. (1986). An unusual Z-system in the obliquely striated muscles of crinoids: three-dimensional structure and computer simulations. *J. Muscle Res. Cell Motil.* **7**, 568-578. doi:10.1007/BF01753572

Cerri, P. S. and Sasso-Cerri, E. (2003). Staining methods applied to glycol methacrylate embedded tissue sections. *Micron* **34**, 365-372. doi:10.1016/S0968-4328(03)00098-2

Chantler, P. D. (1983). Biochemical and structural aspects of molluscan muscle. In *The Mollusca, Vol. 4, Physiology, Part 1* (ed. A.S.M. Saleuddin and K.M. Wilbur), pp. 1-33. New York: Academic Press.
Chapman, G. (1950). Of the movement of worms. *J. Exp. Biol.* **37**, 29-39. doi:10.1242/jeb.27.1.29
Clark, R. B. and Cowey, J. B. (1958). Factors controlling the change of shape of certain nemertean and turbellarian worms. *J. Exp. Biol.* **35**, 731-748. doi:10.1242/jeb.35.4.731
Cloney, R. A. and Brocco, S. L. (1983). Chromatophore organs, reflector cells, iridocytes and leucophores in cephalopods. *Amer. Zool.* **23**, 581-592. doi:10.1093/icb/23.3.581
De Eguileor, M. and Valvassori, R. (1977). Studies on the helical and paramyosinic muscles. VII. Fine structure of body wall muscles in *Sipunculus nudus*. *J. Submicrosc. Cytol.* **9**, 363-372.
Di Clemente, A., Maiole, F., Bornia, I. and Zullo, L. (2021). Beyond muscles: role of intramuscular connective tissue elasticity and passive stiffness in octopus arm muscle function. *J. Exp. Biol.* **224**, jeb242644. doi:10.1242/jeb.242644
Eakin, R. M. and Brandenburger, J. L. (1974). Ultrastructural features of a Gordian worm (Nematomorpha). *J. Ultrastruct. Res.* **46**, 351-374. doi:10.1016/S0022-5320(74)90062-8
Gerry, S. P. and Ellerby, D. J. (2011). Serotonin modulates muscle function in the medicinal leech *Hirudo verbana*. *Biol. Lett.* **7**, 885-888. doi:10.1098/rsbl.2011.0303
Gidmark, N. J., Konow, N., Lopresti, E. and Brainerd, E. L. (2013). Bite force is limited by the force-length relationship of skeletal muscle in black carp, *Mylopharyngodon piceus*. *Biol. Lett.* **9**, 20121181. doi:10.1098/rsbl.2012.1181
Gilly, W. F., Renken, C., Rosenthal, J. J. C. and Kier, W. M. (2020). Specialization for rapid excitation in fast squid tentacle muscle involves action potentials absent in slow arm muscle. *J. Exp. Biol.* **223**, jeb218081. doi:10.1242/jeb.218081
Hanassy, S., Botvinnik, A., Flash, T. and Hochner, B. (2015). Stereotypical reaching movements of the octopus involve both bend propagation and arm elongation. *Bioinspir. Biomim.* **10**, 035001. doi:10.1088/1748-3190/10/3/035001
Hanson, J. and Lowy, J. (1957). Structure of smooth muscles. *Nature* **180**, 906-909. doi:10.1038/180906a0
Hanson, J. and Lowy, J. (1960). Structure and function of the contractile apparatus in the muscles of invertebrate animals. In *Structure and Function of Muscle*, Vol. 1 (ed. G. H. Bourne), pp. 265-335. New York: Academic Press.
Hanson, J. and Lowy, J. (1961). The structure of the muscle fibres in the translucent part of the adductor of the oyster, *Crassostrea angulata*. *Proc. R. Soc. B Biol. Sci.* **154**, 173-196. doi:10.1098/rspb.1961.0027
Harris, J. E. and Crofton, H. D. (1957). Structure and function in the nematodes: internal pressure and cuticular structure in *Ascaris*. *J. Exp. Biol.* **34**, 116-130. doi:10.1242/jeb.34.1.116
Hidaka, T., Kuriyama, H. and Yamamoto, T. (1969). The mechanical properties of the longitudinal muscle in the earthworm. *J. Exp. Biol.* **50**, 431-443. doi:10.1242/jeb.50.2.431
Hill, A. V. (1938). The heat of shortening and the dynamic constants of muscle. *Proc. R. Soc. B Biol. Sci.* **126**, 136-195. doi:10.1098/rspb.1938.0050
Hooper, S. L. and Thuma, J. B. (2005). Invertebrate muscles: muscle specific genes and proteins. *Physiol. Rev.* **85**, 1001-1060. doi:10.1152/physrev.00019.2004
Josephson, R. K. (1975). Extensive and intensive factors determining the performance of striated muscle. *J. Exp. Zool.* **194**, 135-153. doi:10.1002/jez.1401940109
Kasamatsu, C., Kimura, S., Kagawa, M. and Hatae, K. (2004). Identification of high molecular weight proteins in squid muscle by western blotting analysis and postmortem rheological changes. *Biosci. Biotechnol. Biochem.* **68**, 1119-1124. doi:10.1271/bbb.68.1119
Kennedy, E. B. L., Buresch, K. C., Boinapally, P. and Hanlon, R. T. (2020). Octopus arms exhibit exceptional flexibility. *Sci. Rep.* **10**, 20872. doi:10.1038/s41598-020-77873-7
Kier, W. M. (1982). The functional morphology of squid (Loliginidae) arms and tentacles. *J. Morphol.* **172**, 179-192. doi:10.1002/jmor.1051720205
Kier, W. M. (1985). The musculature of squid arms and tentacles: ultrastructural evidence for functional differences. *J. Morphol.* **185**, 223-239. doi:10.1002/jmor.1051850208
Kier, W. M. (1989). The fin musculature of cuttlefish and squid (Mollusca, Cephalopoda): Morphology and mechanics. *J. Zool.* **217**, 23-38. doi:10.1111/j.1469-7998.1989.tb02472.x
Kier, W. M. (1991). Squid cross-striated muscle: the evolution of a specialized muscle fiber type. *Bull. Mar. Sci.* **49**, 389-403.
Kier, W. M. (1996). Muscle development in squid: ultrastructural differentiation of a specialized muscle fiber type. *J. Morphol.* **229**, 271-288. doi:10.1002/(SICI)1097-4687(199609)229:3<271::AID-JMOR3>3.0.CO;2-1
Kier, W. M. (2012). The diversity of hydrostatic skeletons. *J. Exp. Biol.* **215**, 1247-1257. doi:10.1242/jeb.056549
Kier, W. M. (2016). The musculature of coleoid cephalopod arms and tentacles. *Front. Cell Dev. Biol.* **4**, 10. doi:10.3389/fcell.2016.00010
Kier, W. M. and Curtin, N. A. (2002). Fast muscle in squid (*Loligo pealei*): contractile properties of a specialized muscle fibre type. *J. Exp. Biol.* **205**, 1907-1916. doi:10.1242/jeb.205.13.1907
Kier, W. M. and Smith, K. K. (1985). Tongues, tentacles and trunks: The biomechanics of movement in muscular-hydrostats. *Zool. J. Linn. Soc.* **83**, 307-324. doi:10.1111/j.1096-3642.1985.tb01178.x
Kier, W. M. and Stella, M. P. (2007). The arrangement and function of octopus arm musculature and connective tissue. *J. Morph.* **268**, 831-843. doi:10.1002/jmor.10548
Kier, W. M. and Thompson, J. T. (2003). Muscle arrangement, function and specialization in recent coleoids. *Berliner Paläobiologische Abhandlungen* **3**, 141-162.
Kier, W. M. and Van Leeuwen, J. L. (1997). A kinematic analysis of tentacle extension in the squid *Loligo pealei*. *J. Exp. Biol.* **200**, 41-53. doi:10.1242/jeb.200.1.41
Kier, W. M., Smith, K. K. and Miyan, J. A. (1989). Electromyography of the fin musculature of the cuttlefish, *Sepia officinalis*. *J. Exp. Biol.* **143**, 17-31. doi:10.1242/jeb.143.1.17
Kuga, H. and Matsuno, A. (1988). Ultrastructural investigations on the anterior adductor muscle of a brachipoda, *Lingula unguis*. *Cell Struct. Funct.* **13**, 271-279. doi:10.1247/csf.13.271
Kuznetsova, A., Brockhoff, P. B. and Christensen, R. H. B. (2017). lmerTest package: tests in linear mixed effects models. *J. Stat. Softw.* **82**, 1-26. doi:10.18637/jss.v082.i13
Lanzavecchia, G. (1977). Morphological modulations in helical muscles (Aschelminthes and Annelida). *Int. Rev. Cytol.* **51**, 133-186. doi:10.1016/S0074-7696(08)60227-2
Lanzavecchia, G. (1985). Superelongation in helical muscles of leeches. *J. Muscle Res. Cell Motil.* **6**, 569-584.
Lanzavecchia, G. and Arcidiacono, G. (1981). Contraction mechanism of helical muscles: experimental and theoretical analysis. *J. Submicrosc. Cytol.* **13**, 253-266.
Lanzavecchia, G. and De Eguileor, M. (1976). Studies on the helical and paramyosinic muscles. Part V. *J. Submicrosc. Cytol.* **8**, 69-88.
Lanzavecchia, G., De Eguileor, M. and Valvassori, R. (1985). Superelongation in helical muscles of leeches. *J. Muscle Res. Cell Motil.* **6**, 569-584. doi:10.1007/BF00711915
Layland, J., Young, I. S. and Altringham, J. D. (1995). The length dependence of work production in rat papillary muscles *in vitro*. *J. Exp. Biol.* **198**, 2491-2499. doi:10.1242/jeb.198.12.2491
Levy, G., Flash, T. and Hochner, B. (2015). Arm coordination in octopus crawling involves unique motor control strategies. *Curr. Biol.* **25**, 1195-1200. doi:10.1016/j.cub.2015.02.064
Lieber, R. L. and Ward, S. R. (2011). Skeletal muscle design to meet functional demands. *Phil. Trans. R. Soc. B Biol. Sci.* **366**, 1466-1476. doi:10.1098/rstb.2010.0316
Lowy, J. and Mulvany, M. J. (1973). Mechanical properties of guinea pig taenia coli muscles. *Acta Physiol. Scand.* **88**, 123-136. doi:10.1111/j.1748-1716.1973.tb05439.x
Margheri, L., Laschi, C. and Mazzolai, B. (2012). Soft robotic arm inspired by the octopus: I. From biological functions to artificial requirements. *Bioinspir. Biomim.* **7**, 025004. doi:10.1088/1748-3182/7/2/025004
Marsh, R. L. and Olson, J. M. (1994). Power output of scallop adductor muscle during contractions replicating the *in vivo* mechanical cycle. *J. Exp. Biol.* **193**, 139-156. doi:10.1242/jeb.193.1.139
Matsuno, A. and Kuga, H. (1989). Ultrastructure of muscle cells in the adductor of the boring clam *Tridacna crocea*. *J. Morphol.* **200**, 247-253. doi:10.1002/jmor.1052000303
Mazzolai, B., Margheri, L., Dario, P. and Laschi, C. (2013). Measurements of octopus arm elongation: Evidence of differences by body size and gender. *J. Exp. Mar. Biol. Ecol.* **447**, 160-164. doi:10.1016/j.jembe.2013.02.025
Miller, J. B. (1975). The length-tension relationship of the dorsal longitudinal muscle of a leech. *J. Exp. Biol.* **62**, 43-53. doi:10.1242/jeb.62.1.43
Milligan, B. J., Curtin, N. A. and Bone, Q. (1997). Contractile properties of obliquely striated muscle from the mantle of squid (*Alloteuthis subulata*) and cuttlefish (*Sepia officinalis*). *J. Exp. Biol.* **200**, 2425-2436. doi:10.1242/jeb.200.18.2425
Millman, B. M. (1967). Mechanism of contraction in molluscan muscle. *Am Zool.* **7**, 583-591. doi:10.1093/icb/7.3.583
Nesher, N., Maiole, F., Shomrat, T., Hochner, B. and Zullo, L. (2019). From synaptic input to muscle contraction: arm muscle cells of *Octopus vulgaris* show unique neuromuscular junction and excitation–contraction coupling properties. *Proc. R. Soc. B Biol. Sci.* **286**, 20191278. doi:10.1098/rspb.2019.1278
Nicaise, G. and Amsellem, J. (1983). Cytology of muscle and neuromuscular junction. In *The Mollusca, Vol. 4, Physiology, Part 1* (ed. A.S.M. Saleuddin and K.M. Wilbur), pp. 1-33. New York: Academic Press.
Norenburg, J. L. and Roe, P. (1998). Observations on musculature in pelagic nemerteans and on pseudostriated muscle in nemerteans. *Hydrobiologia* **356**, 109-120.

Nunzi, M. G. and Franzini-Armstrong, C. (1981). The structure of smooth and striated portions of the adductor muscle of the valves in a scallop. *J. Ultrastruct. Res.* **76**, 134-148. doi:10.1016/S0022-5320(81)80012-3
Olson, J. M. and Marsh, R. L. (1993). Contractile properties of the striated adductor muscle in the bay scallop *Argopecten irradians* at several temperatures. *J. Exp. Biol.* **176**, 175-193. doi:10.1242/jeb.176.1.175
Olszewski-Jubelirer, J. (2015). Obliquely-striated muscle is not just for super-elongation. *MSc thesis*, University of North Carolina, Chapel Hill.
Ort, C. A., Kristan, W. B. and Stent, G. S. (1974). Neuronal control of swimming in the medicinal leech. *J. Comp. Physiol.* **94**, 121-154. doi:10.1007/BF00617838
Page, S. G. and Huxley, H. E. (1963). Filament lengths in striated muscle. *J. Cell Biol.* **19**, 369-390. doi:10.1083/jcb.19.2.369
Paps, J., Baguñà, J. and Riutort, M. (2009). Lophotrochozoa internal phylogeny: new insights from an up-to-date analysis of nuclear ribosomal genes. *Proc. R. Soc. B Biol. Sci.* **276**, 1245-1254. doi:10.1098/rspb.2008.1574
Prosser, C. L. (1979). Evolution and diversity of nonstriated muscles. In *Handbook of Physiology, Cardiovascular System II.* (ed. D. Bohr), pp. 635-670. Bethesda, MD: American Physiology Society.
Prosser, C. L. (1982). Diversity of narrow-fibered and wide-fibered muscles. In *Basic Biology of Muscles: A Comparative Approach* (ed. B.M. Twarog, R. J. C. Levine and M. M. Dewey), pp. 381-397. NY: Raven Press.
Rack, P. M. H. and Westbury, D. R. (1969). The effects of length and stimulus rate on tension in the isometric cat soleus muscle. *J. Physiol.* **204**, 443-460. doi:10.1113/jphysiol.1969.sp008923
Reynolds, E. (1963). The use of lead citrate at high pH as an electron-opaque stain in electron microscopy. *J. Cell Biol.* **17**, 208-212. doi:10.1083/jcb.17.1.208
Rieger, R. M. and Mainitz, M. (1977). Comparative fine structure study of the body wall in Gnathostomulida and their phylogenetic position between Platyhelminthes and Aschelminthes. *J. Zool. Syst. Evol.* **15**, 9-35. doi:10.1111/j.1439-0469.1977.tb00530.x
Rieger, R. M., Ruppert, E., Rieger, G. E. and Schoepfer-Sterrer, C. (1974). On the fine structure of gastrotrichs with description of *Chordodasys antennatus* sp. n. *Zool. Script.* **3**, 219-237. doi:10.1111/j.1463-6409.1974.tb00819.x
Rogers, C. M., Nelson, L., Milligan, B. J. and Brown, E. R. (1997). Different excitation-contraction coupling mechanisms exist in squid, cuttlefish, and octopod mantle muscle. *J. Exp. Biol.* **200**, 3033-3041. doi:10.1242/jeb.200.23.3033
Rokni, D. and Hochner, B. (2002). Ionic currents underlying fast action potentials in the obliquely striated muscle cells of the octopus arm. *J. Neurophysiol.* **88**, 3386-3397. doi:10.1152/jn.00383.2002
Rosenbluth, J. (1965). Ultrastructural organization of obliquely striated muscle fibers in *Ascaris lumbricoides*. *J. Cell Biol.* **25**, 495-515. doi:10.1083/jcb.25.3.495
Rosenbluth, J. (1967). Obliquely striated muscle. III. Contraction mechanism of *Ascaris* body muscle. *J. Cell Biol.* **34**, 15-33. doi:10.1083/jcb.34.1.15
Rosenbluth, J. (1968). Obliquely striated muscle. IV. Sarcoplasmic reticulum, contractile apparatus, and endomysium of the body muscle of a polychaete, *Glycera*, in relation to its speed. *J. Cell Biol.* **36**, 245-259. doi:10.1083/jcb.36.1.245
Rosenbluth, J. (1972). Obliquely striated muscle. In *The Structure and Function of Muscle*, Vol. 1, 2nd edn. (ed. G. H. Bourne), pp. 389-420. NY: Academic Press.
Rosenbluth, J., Szent-Györgyi, A. G. and Thompson, J. T. (2010). The ultrastructure and contractile properties of a fast-acting, obliquely striated, myosin-regulated muscle: the funnel retractor of squids. *J. Exp. Biol.* **213**, 2430-2443. doi:10.1242/jeb.037820
Rubenson, J., Pires, N. J., Loi, H. O., Pinniger, G. J. and Shannon, D. G. (2012). On the ascent: the soleus operating length is conserved to the ascending limb of the force-length curve across gait mechanics in humans. *J. Exp. Biol.* **215**, 3539-3551. doi:10.1242/jeb.070466
Ruppert, E. E. (1991). Gastrotricha. In *Microscopic Anatomy of Invertebrates. Vol. 4: Aschelminthes* (ed. F. W. Harrison and E. E. Ruppert), pp. 41-109. Wiley-Liss, Inc.
Schneider, C. A., Rasband, W. S. and Eliceiri, K. W. (2012). NIH Image to ImageJ: 25 years of image analysis. *Nat. Methods* **9**, 671-675. doi:10.1038/nmeth.2089
Shadwick, R. E. (2008). Foundations of animal hydraulics: geodesic fibres control the shape of soft bodied animals. *J. Exp. Biol.* **211**, 289-291. doi:10.1242/jeb.008912
Shaffer, J. F. and Kier, W. M. (2016). Tuning of shortening speed in coleoid cephalopod muscle: no evidence for tissue-specific muscle myosin heavy chain isoforms. *Invert. Biol.* **135**, 3-12. doi:10.1111/ivb.12111
Tashiro, N. (1971). Mechanical properties of the longitudinal and circular muscle in the earthworm. *J. Exp. Biol.* **55**, 101-110. doi:10.1242/jeb.55.1.101
Tashiro, N. and Yamamoto, T. (1971). The phasic and tonic contraction in the longitudinal muscle of the earthworm. *J. Exp. Biol.* **55**, 111-122. doi:10.1242/jeb.55.1.111
Taylor-Burt, K. R., Kier, W. M., Olszewski-Jubelirer, J. and Thompson, J. T. (2018). Shape, size and structure affect obliquely striated muscle function in squid. *Integ. Comp. Biol.* **58**, 261-275. doi:10.1093/icb/icy053
Teuchert, G. (1974). Aufbau und Feinstruktur der Muskelsysteme von *Turbanella cornuta* Remane (Gastrotricha, Macrodasyoidea). *Mikrofauna d. Meeresb.* **39**, 1-26.
Thompson, J. T. and Kier, W. M. (2006). Ontogeny of circular muscle ultrastructure and implications for jet locomotion in Oval Squid, *Sepioteuthis lessoniana*. *J. Exp. Biol.* **209**, 433-443. doi:10.1242/jeb.02017
Thompson, J. T., Szczepanski, J. A. and Brody, J. (2008). Mechanical specialization of the obliquely striated circular mantle muscle fibres of the long-finned squid *Doryteuthis pealeii*. *J. Exp. Biol.* **211**, 1463-1474. doi:10.1242/jeb.017160
Thompson, J. T., Bartol, I. K., Baksi, A. E., Li, K. Y. and Krueger, P. S. (2010). The ontogeny of muscle structure and locomotory function in the long-finned squid *Doryteuthis pealeii*. *J. Exp. Biol.* **213**, 1079-1091. doi:10.1242/jeb.034553
Thompson, J. T., Shelton, R. M. and Kier, W. M. (2014). The length-force behavior and operating length range of squid muscle vary as a function of position in the mantle wall. *J. Exp. Biol.* **217**, 2181-2192. doi:10.1242/jeb.083907
Thompson, J. T., Lavalva, S. M. and Loiacono, M. M. (2016). A multi-function muscle in squid. *Biol. Bull.* **231**, 225-235. doi:10.1086/691070
Toida, N., Kuriyama, H., Tashiro, N. and Ito, Y. (1975). Obliquely striated muscle. *Physiol. Rev.* **55**, 700-756. doi:10.1152/physrev.1975.55.4.700
Tu, M. S. and Daniel, T. L. (2004). Cardiac-like behavior of an insect flight muscle. *J. Exp. Biol.* **207**, 2455-2464. doi:10.1242/jeb.01039
Turbeville, J. M. and Ruppert, E. E. (1985). Comparative ultrastructure and the evolution of nemertines. *Am. Zool.* **25**, 53-71. doi:10.1093/icb/25.1.53
Ward, S. M., McKerr, G. and Allen, J. M. (1986). Structure and ultrastructure of muscle systems within *Grillotia erinaceus* metacestodes (Cestoda, Trypanorhyncha). *Parasitology.* **93**, 587-597. doi:10.1017/S0031182000081294
Winegrad, S. (1974). Resting sarcomere length-tension relation in living frog heart. *J. Gen. Physiol.* **64**, 343-355. doi:10.1085/jgp.64.3.343
Williams, C. D., Salcedo, M. K., Irving, T. C., Regnier, M. and Daniel, T. L. (2013). The length-tension curve in muscle depends on lattice spacing. *Proc. R. Soc. B Biol. Sci.* **280**, 20130697. doi:10.1098/rspb.2013.0697
Zullo, L., Di Clemente, A. and Maiole, F. (2022). How octopus arm muscle contractile properties and anatomical organization contribute to arm functional specialization. *J. Exp. Biol.* **225**, jeb243163. doi:10.1242/jeb.243163

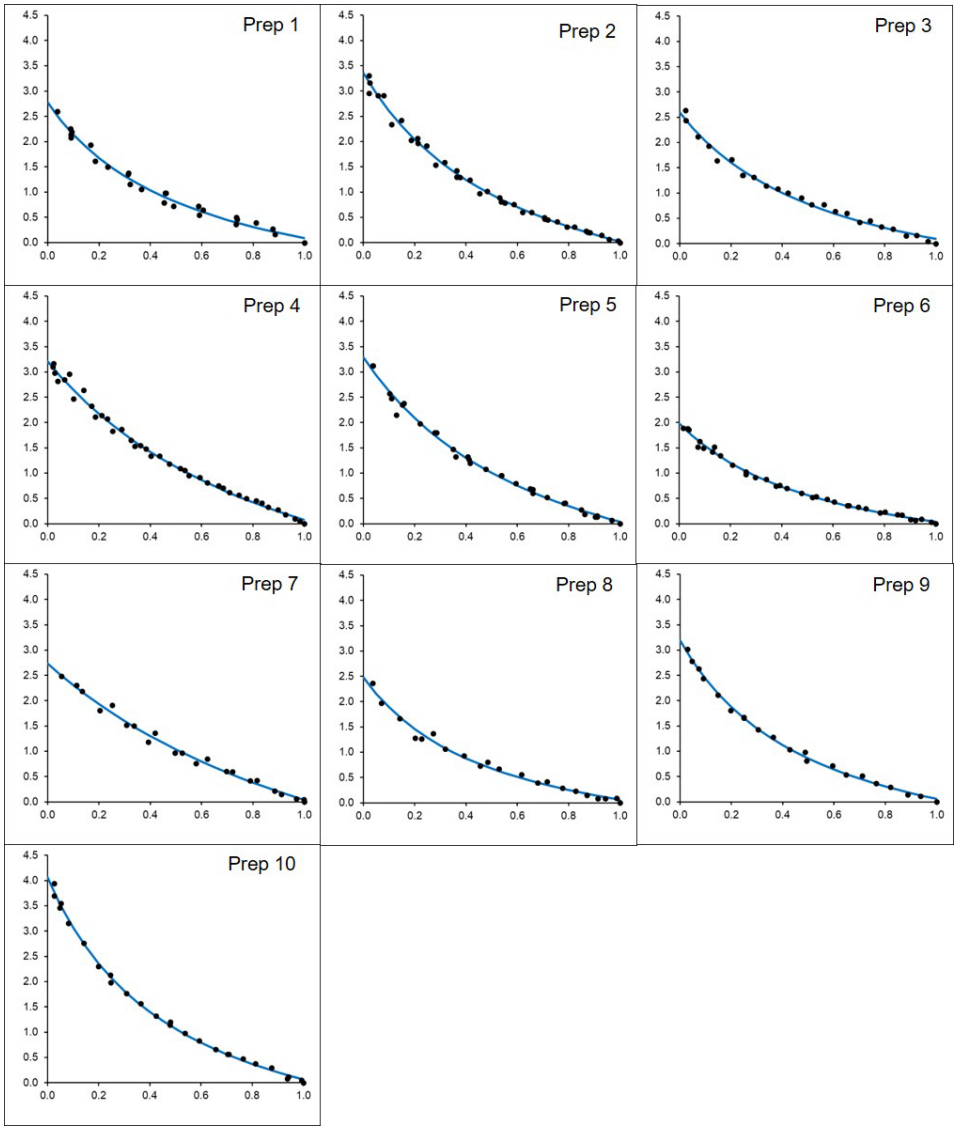

Fig. S1. Force-velocity plots. The vertical axes are shortening velocity in L_0 s-1, where L_0 is preparation length at which maximum isometric force was produced. The horizontal axes are force relative to P_0 (i.e., the maximum isometric force). Each plot contains the raw data (black circles) and the single hyperbolic fit (blue lines). The preparation (Prep) numbers correspond to those listed in Table 1 in the text.

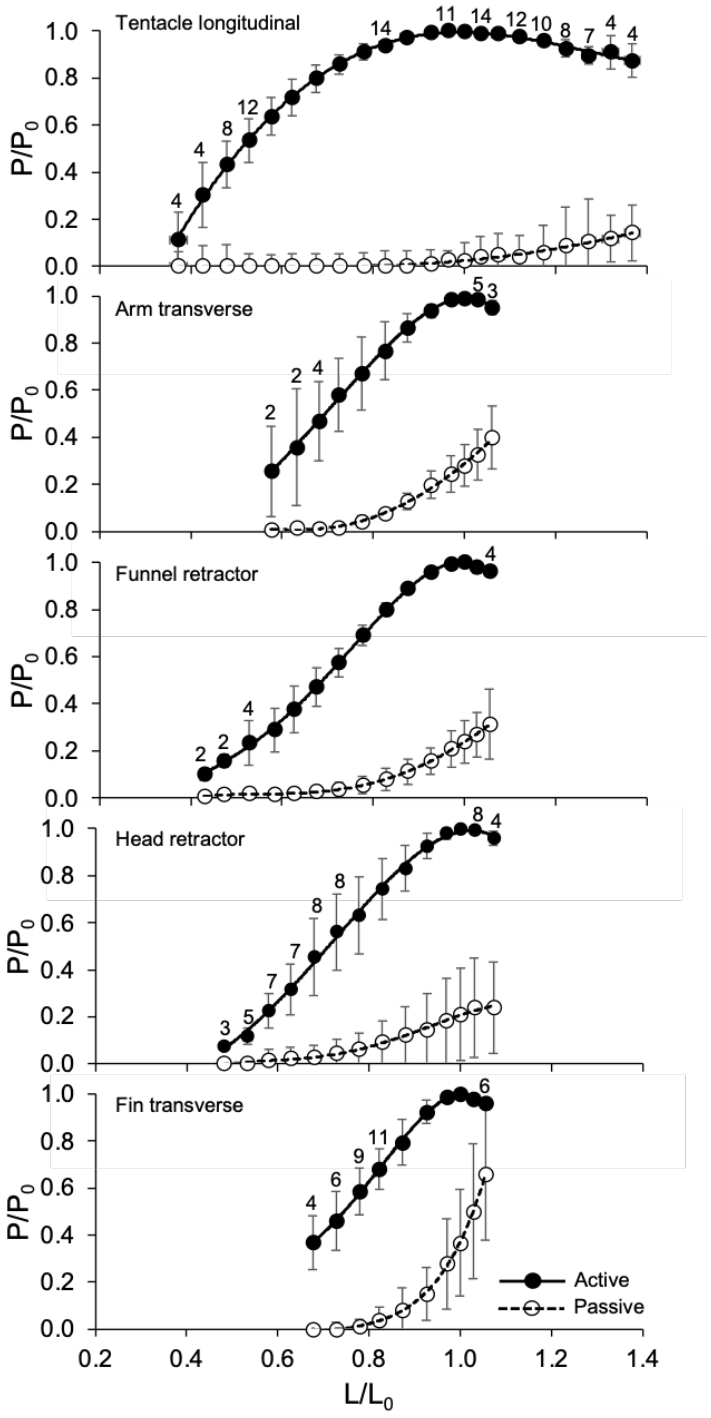

Fig. S2. Active (closed circles) and passive (open circles) force-length relationships by muscle (as in Fig. 6, tentacle longitudinal n=15, arm transverse n=6, funnel retractor n=6, head retractor n=9, fin transverse n=13). Curves are 4th order polynomial fits to averaged data. Averages were calculated by binning data by 0.05L_0 intervals. Sample sizes for points that do not include data from all preps are noted above the points on the active curves. Error bars represent standard deviation in relative force (vertical) and length (horizontal) for each bin.

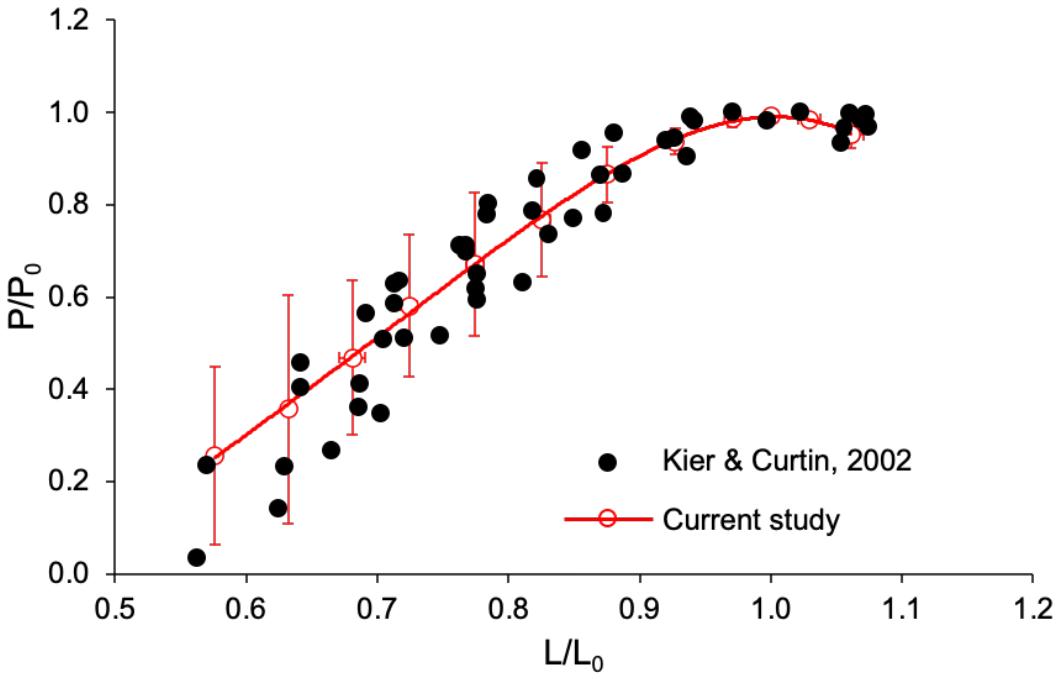

Fig. S3. Length-force data for arm transverse muscle preparations from the current study (red, open circles) and Kier & Curtin (2002) (black, closed circles). Preparations from the current study were dissected from 300-µm thick cross-sectional slices of the third arm (obtained with a vibratome), tied to transducer loops (see below for detail), and stimulated at 150 Hz (2 ms pulse width, 100 ms duration). The preparations from Kier and Curtin (2002) were dissected from approximately 1-mm thick cross-sectional slabs of the third arm, glued to T-shaped aluminum foil clips, and stimulated at 50 Hz (2 ms pulse width, 100 ms duration). Despite methodological differences, the previously published data for arm transverse fibers closely matches the observations from the current study. (Modified from Kier & Curtin, 2002.)

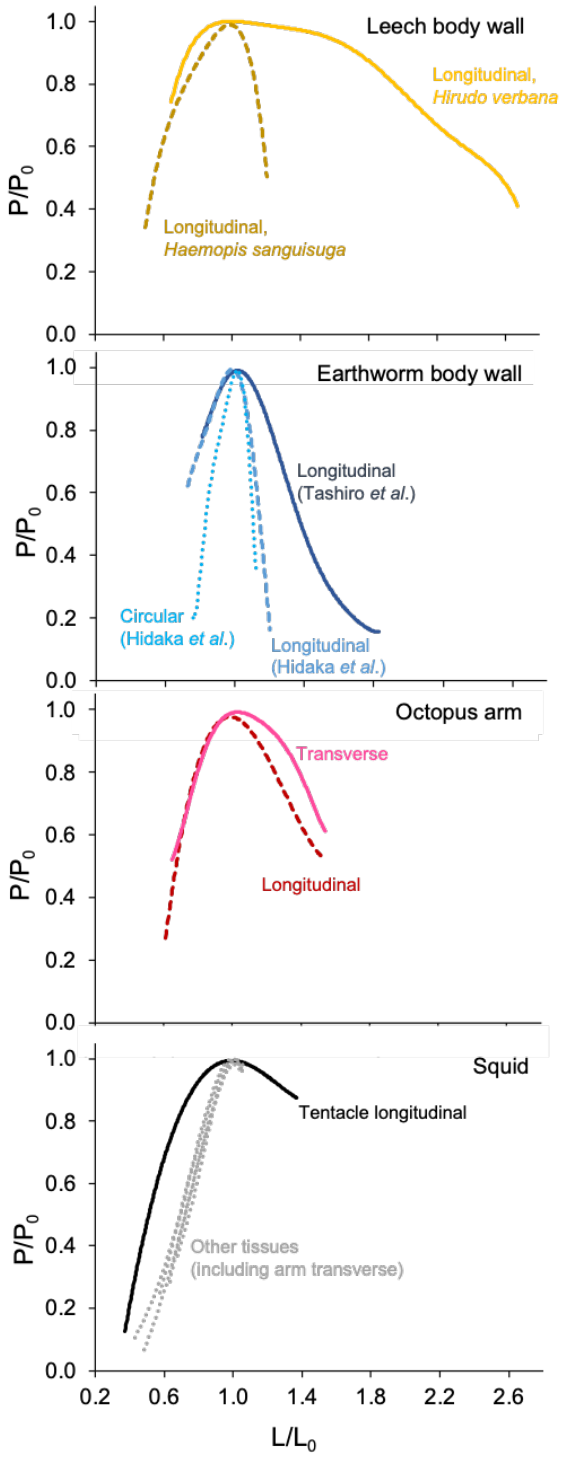

Fig. S4. Length-force relationships as in Fig. 7 plotted by type of animal for clarity. Panels include labels for animal and structure, except the squid panel, which includes data from various tissues [solid black: tentacle longitudinal, dashed gray: includes arm transverse, fin transverse, funnel retractor, head retractor, and mantle inner circular fibers (from Thompson *et al.,* 2014)]. Squid curves are polynomial fits for averaged data while the rest are digitized from previously published curves. The breadth of length-force relationships of obliquely striated muscles varies both within and among species. Source data and species are: Squid: *Doryteuthis pealeii*, current study and Thompson *et al.,* 2014; Octopus: Zullo *et al.,* 2022, *Octopus vulgaris*; Leech: Gerry & Ellerby, 2011, *Hirudo verbana*; Miller, 1975, *Haemopis sanguisuga*; Tashiro and Yamamoto, 1971, and Hidaka *et al.,* 1969, *Pheretima communissima*.

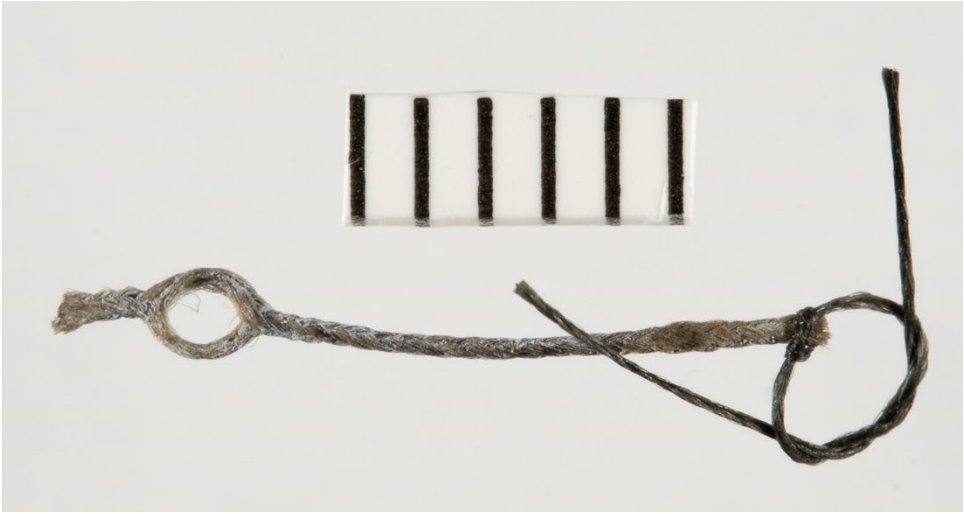

Fig. S5. Transducer loop. See Supplemental Information text for additional details. Millimeter ruler for scale.

Supplementary Materials and Methods

ADDITIONAL DETAIL ABOUT THE METHODS:

Transducer loops

The "transducer loops" (see Fig. S5) were made from a short length of 3/0 surgical silk suture (Fine Science Tools, Foster City, CA, USA). We placed the silk on a Sylgard-lined petri dish, and then used fine forceps and Number 00 insect pins (Fine Science Tools) to carefully separate the finely braided silk threads from each other to create a small hole. The hole was enlarged and held open by inserting a T-shaped stainless-steel dissection pin (0.9 mm diameter) through the hole and into the Sylgard. Tiny amounts of Vetbond were then applied with the tip of an insect pin to the threads surrounding the hole to fix the threads in place, and then the dish was flooded with water to cure the glue. Immediately after curing, we used forceps to carefully separate the silk loops from the dissection pin; delaying this process for more than a few minutes resulted in firm attachment of the loop to the pin.

Once the glue cured, we cut the transducer loop so that its total length was 5-8 mm (the loop plus a short length of suture material). A 10-cm length of 6/0 surgical silk was then tied near the tip with a single surgical knot and fixed in place with a tiny drop of Vetbond. We next pinned a transducer loop to a Sylgard-lined petri dish filled with chilled fresh squid saline and gently aligned one end of the muscle preparation to the long axis of the loop. About 1 mm of the end of the preparation extended past the location of the 6/0 surgical silk. The length of 6/0 surgical silk was then knotted (surgeon's knot) around the preparation to secure it snugly to the transducer loop (Fig. 2F).

This procedure was repeated with a second transducer loop for the other end of the muscle preparation. Once both transducer loops were secured, the water was drained from the dish and the ends of the preparation that extended past the 6/0 silk (i.e., the free ends; see white arrow in Fig. 2F) were gently blotted dry with small pieces of Kimwipes (Kimberly-Clark, Inc., Roswell, GA, USA) that had been twisted into fine swabs. A tiny droplet of Vetbond was then applied to each free end of the tissue, and the dish flooded with chilled squid saline to cure the glue. Dabbing the tips of the free ends of the muscle preparations with Vetbond created a rigid structure that could not easily slide past the knotted 6/0 surgical silk once the muscle preparation experienced tensile loads. Moreover, it allowed us to tie the muscle preparation to the transducer loop snugly but without applying so much force to the preparation that it was prone to ripping at the knots.

SUPPLEMENTARY REFERENCES:

Gerry, S.P. and Ellerby, D.J. (2011). Serotonin modulates muscle function in the medicinal leech *Hirudo verbana. Biol. Lett.* **7,** 885-888. doi:10.1098/rsbl.2011.0303.

Hidaka, T., Kuriyama, H., and Yamamoto, T. (1969). The mechanical properties of the longitudinal muscle in the earthworm. *J. Exp. Biol.* **50,** 431-443.

Kier, W.M. and Curtin, N.A. (2002). Fast muscle in squid (*Loligo pealei*): contractile properties of a specialized muscle fibre type. *J. Exp. Biol.* **205,** 1907-1916.

Miller, J.B. (1975). The length-tension relationship of the dorsal longitudinal muscle of a leech. *J. Exp. Biol.* **62**, 43-53.

Tashiro, N. and Yamamoto, T. (1971). The phasic and tonic contraction in the longitudinal muscle of the earthworm. *J. Exp. Biol.* **55,** 111-122.

Thomspon, J.T., Shelton, R.M., and Kier, W.M. (2014). The length-force behavior and operating length range of squid muscle vary as a function of position in the mantle wall. *J. Exp. Biol.* **217,** 2181-2192. doi:10.1242/jeb.083907.

Zullo, L., Di Clemente, A., and Maiole, F. (2022). How octopus arm muscle contractile properties and anatomical organization contribute to arm functional specialization. *J. Exp. Bio.* **225,** jeb243163. doi:10.1242/jeb.24363.